NASA Contractor Report 3367

Measurements of Laminar and Turbulent Flow in a Curved Duct With Thin Inlet Boundary Layers

A. M. K. P. Taylor, J. H. Whitelaw,
and M. Yianneskis

NASA

NASA Contractor Report 3367

Measurements of Laminar and Turbulent Flow in a Curved Duct With Thin Inlet Boundary Layers

A. M. K. P. Taylor, J. H. Whitelaw,
and M. Yianneskis
Imperial College of Science and Technology
London, England

NASA

National Aeronautics
and Space Administration

Scientific and Technical
Information Branch

1981

TABLE OF CONTENTS

SUMMARY

The secondary flows in a 90° square bend of 40 mm hydraulic diameter and mean radius of 92 mm have been measured at Reynolds numbers of 790 and 40 000 in a water tunnel. The boundary layers at the inlet to the bend were approximately 25% and 15% of the hydraulic diameter respectively. The results provide a better understanding of the two flows, are compared with published data of the flow with fully developed profiles at the bend inlet and will assist the evaluation of numerical prediction techniques. Laser-Doppler velocimetry was used to measure velocities in the plane of curvature and, in the turbulent flow, to measure the associated fluctuations and cross-correlations. Data is also given for stations upstream and downstream of the bend. For turbulent flow, wall pressure distributions are reported.

In the laminar flow strong streamwise vorticity is generated on entry to the bend, with the result that the locus of maximum streamwise velocity on the symmetry plane moves towards the outer radius and regions of high streamwise velocity are convected along the sidewalls. In the turbulent flow, smaller secondary motions at the inlet initially allow this locus to move towards the inner radius under the action of pressure gradients before the influence of the strengthening secondary motion becomes evident about 60° around the bend. The difference in the behaviour of the secondary motion is related to the difference in thickness of the inlet boundary layers.

Comparison with data for fully-developed profiles at inlet shows that the differences from the present laminar flow are of detail. In the turbulent flow, the influence of the secondary motion is apparent at earlier streamwise positions for the fully-developed profile. The turbulent fields show qualitative similarities, such as higher shear stress towards the outer radius and large anisotropy at the exit from the bend. Quantitatively, the turbulent levels in the present flow are much smaller, as expected.

The measurements are presented in tabular form and are also available on magnetic tape for ease of comparison with predictions.

1

1. INTRODUCTION

Flows in curved ducts are found in a wide range of practical configurations and, in this report, they are discussed in the context of a 90° bend of square cross-section and comparatively strong curvature. A distinguishing characteristic of such flows is the generation of streamwise vorticity, or "secondary motion", within the duct which can result in large redistributions of, for example, the streamwise velocities. The change in the flow on passing through the duct can be sufficient to impair the performance of plant downstream of the duct, for example the performance of the compressor in a curved aircraft intake duct.

Information on the flow in bends has been considered in reference 1 and, with the exception of a few measurements of local velocity in bends of square cross-section, relates to pressure characteristics. Local measurements have been obtained for laminar flows in the round ducts of references 2 and 3 and in the square duct of reference 4 which also yielded heat-transfer information. Turbulent flow measurements have been reported in reference 5 for a near two-dimensional channel and in reference 6 for a channel with an aspect ratio of 2. The maximum ratio of cross-stream to bulk velocity was found, in reference 3, to be of the order of 0.5 and for the turbulent flow of reference 6 to be of the order of 0.3. The measurements of references 7 and 8 provide the most comprehensive velocity information for laminar and turbulent flow in a square duct with strong curvature. The flow approaching the bend was fully developed for both the laminar and turbulent flows and the development of the velocity through the ducts was markedly different in the two cases.

The duct geometry investigated in this report is identical to that of references 7 and 8,with thin inlet boundary layers at the entrance to the bend. This condition is relevant to the case of aircraft intake ducts. Measurements of the velocity characteristics within the duct are reported for both laminar and turbulent flow and provide a basis for the understanding of the flow and its development in the two flow regimes. The thickness of the boundary layers at the inlet is expected to be important because of the related change in the cross-stream vorticity and this can be quantified by comparison with the results of references 7 and 8. A further purpose is to provide detailed data in a form suitable for the evaluation of numerical prediction techniques and this requires careful measurement of the conditions at the inlet of the duct for use as boundary conditions in the prediction algorithm. The laminar and turbulent flow can be used to study, respectively, the numerical accuracy of the procedure and to provide an assessment of the turbulence model.

The aim of the report is to make available accurate measurements of the streamwise and cross-stream velocity and wall static pressure in sufficient detail to fulfil the purposes of the previous paragraph. In common with the previous investigations of references 7 to 9, laser-Doppler velocimetry was used to measure the velocity components.

2

The following section describes the experimental procedure and includes estimates of the errors associated with the measurements presented in section 3. The results are discussed in section 4 and a summary of conclusions is provided in section 5.

2. EXPERIMENTAL PROCEDURE

2.1 Flow Configuration

The duct was a 90° bend of mean radius 92 mm and of radius ratio 2.3, identical to that of references 7 and 8. The dimensions of the cross-section (40 ± 0.1 x 40 ±0.1 mm) conform closely to those used for the straight square-sectioned duct investigated in reference 9 and used in references 7 and 8 to provide fully-developed flow upstream of the bend. The geometry is illustrated in figure 1, together with the co-ordinate system adopted in the report. The bend was installed in a water tunnel with the plane of symmetry located horizontally. Figure 2 shows a plan view of the water tunnel and the lengths of the straight ducts upstream and downstream of the bend. The flow rate through the bend was controlled by precision-bore flowmeters. The bulk velocities, V_c, were 1.98 cm/s and 1.00 m/s for the laminar and turbulent flows respectively, corresponding to Reynolds numbers, Re, of 790 and 40 000 and Dean numbers, De, of 368 and 18 700. The temperature of the water was maintained at 20° ± 2^oC for all the experiments.

2.2 Velocimeter configuration, Doppler signal processing and measurement technique

Figure 3(i) shows the optical arrangement of the laser-Doppler velocimeter with the sensitivity vector of the velocimeter in the gapwise direction. It is similar to an arrangement described in reference 10 except that frequency shifting of the laser light was not used. Figures 3(ii) and (iii) show photographs of the bend and optical system respectively. The mirror, which was used to turn the optical axis through 90°, was flat to one-tenth of the wavelength of light. The principal characteristics of the optical system are summarised in the following table:

Characteristics of the optical arrangement	Laminar flow	Turbulent flow
Focal length of imaging lens (mm)	300	200
Half-angle of intersection	5.9°	9.3°
Fringe separation (line-pair spacing)	3 μm	2 μm
Number of fringes in measuring volume	52	86
Intersection volume diameter calculated at $1/e^2$ intensity (mm)	0.158	0.167
Intersection volume length calculated at $1/e^2$ intensity (mm)	1.500	1.357
Photomultiplier pinhole diameter (mm)	0.33	0.50
Transform constant (MHz/ms^{-1})	0.324	0.510

The Doppler signals were detected by a photomultiplier tube (E.M.I. 9658B) and demodulated by a frequency tracker (Cambridge Consultants CC01). The voltage analogue of the Doppler frequency was averaged to give a mean and root-mean-square voltage, as indicated in figure 4. For the turbulent flow measurements, the flow was seeded (see reference 11) with minute quantities of milk to increase the scattering particle concentration and thereby increase the particle arrival rate.

The local streamwise (U) and gapwise (V) components of velocity, and for turbulent flow the fluctuating components $\tilde{u}$, $\tilde{v}$ and cross-correlation $\overline{uv}$, were obtained by making measurements of the Doppler frequency in three directions ($0^{\circ}, \pm 45^{\circ}$) relative to the local streamwise direction at each measurement point. The method of data reduction involves resolving these measured frequencies into streamwise and gapwise components as described in reference 9. The third component of velocity, W, and the associated correlations $\tilde{w}$ and $\overline{uw}$ were measured in a similar manner, with the three measurements being made in the X ~ θ plane.

Wall pressure measurements were obtained by means of pressure tappings let into the walls of the duct. Pressure measurements were made with a water-micromanometer. In laminar flow the pressure differences amounted to 20 μm of water and were too small for reliable measurement.

2.3 Accuracy and precision

The following table summarises the estimates of accuracy (systematic error) and precision (random error) associated with each measurement presented in section 3. No corrections have been applied to take account of finite

4

transit time, mean velocity gradient and instrument noise broadening; see reference 11. Only velocity gradients have a significant effect and this has been included in the systematic errors of the table. This accounts for the $2\frac{1}{2}$ and 3% errors associated with non-dimensional mean velocities; the systematic errors away from the region of high velocity gradients are less than 1%.

Measurement errors

Quantity	Systematic error	Random error
X_H	± 0.5 mm	± 0.02 mm
r^*, z^*	± 0.2 mm	± 0.02 mm
θ	$\pm 0.3^O$	$\pm 0.17^O$
ϕ	$\pm 0.05^O$	nil
V_c (laminar)	$\pm 0.8\%$	$\pm 0.8\%$
V_c (turbulent)	$\pm 1/2\%$	$\pm \frac{1}{2}\%$
U/V_c	up to $2\frac{1}{2}\%$	$\pm 1\frac{1}{2}\%$
V/V_c	up to 3%	$\pm 1\frac{1}{2}\%$
W/V_c	up to 3%	$\pm 1\frac{1}{2}\%$
$\tilde{u}/V_c$	up to 3%	± 1 to $\pm 3\%$
$\tilde{v}/V_c$	up to 3%	$\pm 1\frac{1}{2}\%$ to $\pm 5\%$
$\tilde{w}/V_c$	up to 3%	$\pm 1\frac{1}{2}\%$ to $\pm 5\%$
$\overline{uv}/V_c^2$	$\pm 1\frac{1}{2}\%$	$\pm 2\frac{1}{2}\%$ to $\pm 8\frac{1}{2}\%$
$\overline{uw}/V_c$	$\pm 1\frac{1}{2}\%$	$\pm 2\frac{1}{2}\%$ to $\pm 8\frac{1}{2}\%$
k/V_c^2	$\pm 7\%$	$\pm 8\%$

3. RESULTS

3.1 Laminar Flow Results

The laminar nature of the flow was confirmed by extensive visualisation using hydrogen bubbles produced on 0.375 mm Nichrome wires inserted through the pressure tappings. Still and cine photography recordings were made. The photograph presented as figure 5(i) shows the secondary velocity convecting fluid from the pressure (outer) wall along the sidewall to the suction (inner) wall, for Re = 1275. Flow visualisation did not reveal a region of longitudinal recirculation on the pressure wall as was observed in reference 7. Fig. 5(ii) shows the flow at the exit of the bend. The streaklines indicate large secondary motion near the suction surface and its absence along the mean radius of the bend. Near the pressure surface the bubbles are convected by the secondary motion from the symmetry plane to the sidewall. The velocity profiles presented in the following paragraphs quantify the magnitude and extent of this pattern.

Preliminary measurements were obtained to evaluate the symmetry of the flow and to determine the extent to which the bend influenced the flow upstream. It was found that measurements at equivalent locations on either side of the symmetry plane of the duct agreed within the precision of the measurement. There were no discernable trends and the flow may be regarded as symmetric. Profiles of streamwise velocity at X_H = -0.25 and -0.50 showed that the influence of the bend was detectable at the two stations closest to the plane of the bend entrance but was very small and is unlikely to be present at X_H = -0.75.

The development of the streamwise velocity is depicted in figure 6 in a form comparable to that of reference 7. The boundary layers at X_H = -0.25, defined at 95% of the maximum velocity, are a quarter of the hydraulic diameter (40 mm). The same results are presented as isotachs of streamwise velocity in figure 7 for ease of presentation and subsequent discussion. The contours have been drawn using linear interpolation between the measurement points; no extrapolation outside the measured grid has been carried out. The isotachs in figure 7 (i) suggest that the bend has little effect on the flow upstream of the inlet and that as the fluid moves through the bend, figures 7(ii)-(v), high velocities are found near the pressure surfaces and the sidewalls with a corresponding low velocity region adjacent to the suction surface. The development of the streamwise velocity is influenced by the streamwise pressure gradients. Although wall pressures were not measured, the form can be expected to be similar to that calculated in reference 7, which showed that the gradient is strongly adverse over the suction surface for about 45° while it is strongly favourable over the pressure surface for the same region.

The generation of streamwise vorticity is responsible for the convection of high streamwise velocity fluid from the pressure surface along the sidewalls. Figure 8 shows profiles of the gapwise component of secondary velocity, with figure 9 displaying the same information as isotachs. At X_H = -0.25

6

(figure 8(i)), the velocity is small ($0.05V_c$) but directed towards the suction surface of the straight duct. This flow is evidence of a gapwise pressure gradient upstream of the bend. The profiles in the bend confirm that the fluid near the symmetry plane moves away from the suction surface and that fluid near the sidewalls moves towards the suction surface. This results in a secondary flow of the "first kind" (reference 12), which is a strong helical motion near the suction surface. The largest velocities measured occur at $\theta = 60^0$ with values of the order of $0.6V_c$, although the velocity near the symmetry plane and suction surface has decayed and is close to zero. This feature is seen to continue at $\theta = 77.5^0$ and $X_H = 0.25$ and is associated with the accumulation of low streamwise velocity fluid at the suction surface.

Downstream of the bend, figure 7 (vi) shows that the streamwise velocity has decelerated on the pressure side of the duct. Figure 8 (vi) presents the corresponding profile of gapwise velocity which has decreased greatly from the exit plane of the bend and has also reversed direction close to the pressure surface. For this station, the spanwise (W) component of velocity was measured and is presented in figure 10. The secondary flow thus consists of two counter-rotating vortices which is in agreement with the predictions of reference 7, although the predicted values are generally larger over the cross-section. It is associated with the rapid deceleration of streamwise velocity near the pressure surface causing a positive gapwise velocity near the symmetry plane.

The results from which the graphs have been plotted are tabulated in Appendix 1 as Table I.

3.2 Turbulent flow results

As for the laminar flow, symmetry tests were carried out with results similar to those for the laminar flow. The influence of the bend on the flow upstream was again examined and found to be more extensive than for the laminar flow, being present at $X_H = -0.50$ and -0.75.

The development of the streamwise component of velocity is shown in figure 11. As for the laminar flow, the boundary layers are thinner (15% of the hydraulic diameter) than those of reference 8 at the inlet to the bend. Figure 12 shows the corresponding isotachs which, in contrast to laminar flow, are displaced to the suction surface of the duct, upstream of the bend. Measurements showed that this displacement was negligible at $X_H = -0.75$. The fluid near the suction surface continues to accelerate at $\theta = 30^0$ and by $\theta = 60^0$ the influence of the secondary motion on the contour shape is evident and continues to the exit of the bend, with the position of maximum velocity migrating from $r^* \simeq 0.7$ to $r^* \simeq 0.4$.

The profiles of gapwise velocity are presented in figure 13, with the corresponding contours in figure 14. As expected at X_H = -0.25, the velocity is directed towards the suction surface, for the same reasons as in the laminar flow. The streamwise vorticity that is generated within the bend develops more slowly than for the laminar flow, while the positive velocities occur in the region very close to the sidewalls, corresponding to the thin boundary layers. The maximum velocities are again found at θ = 60°, and are about 0.4V_c. In common with the laminar flow, the velocities on the symmetry plane near the suction surface are small, because of the small streamwise velocity in this region.

The wall pressures are presented in figure 15 (i) as p(θ) with r* as parameter and in figure 15 (ii) as p(r*) with θ as parameter. The large radial pressure gradient at the inlet plane confirms the influence of the bend on the upstream duct. Initially an adverse pressure gradient develops on the pressure surface,and a favourable gradient on the suction surface, causing the observed deceleration and acceleration of the fluid near the respective surfaces. These trends are reversed after $\theta \simeq 50°$. Fig. 15 (ii) shows that as, expected, the largest values of gapwise pressure gradient are associated with the large gapwise velocities at θ = 60° and θ = 77.5°. The pressure loss due to the bend is of the order of 0.1 ρV_c^2, which is comparable to the value reported in reference 1 for a similar configuration.

The development downstream of the bend is shown in figures 13 (vi) and 14 (vi). The position of maximum streamwise velocity lies closer to the pressure wall while fluid near the suction wall has accelerated. The gapwise velocity has decayed less than was the case for the laminar flow, and only one sense of circulation is evident at X_H = 2.50. The third component of velocity, W, is presented in figure 16 with the positive velocity direction defined as for laminar flow.

Figure 17 gives contours of the Reynolds stress $\overline{uv}$. Upstream of the bend the values are low, corresponding to the small boundary layer thicknesses. At successive streamwise planes, large values of $\overline{uv}$ are found near the pressure surface and near the sidewalls indicating that momentum transport is large in this region coinciding with large streamwise-velocity gradients. The change in the sign of $\overline{uv}$ is closely associated with changes in the sign of $\partial U/\partial r^*$, at least for the region $z^* \simeq 0.8$. On the suction side of the bend, the shear stress is generally small except for θ = 60°.

Figures 18 and 19 show the corresponding development of $\tilde{u}$ and $\tilde{v}$. Initially, high values are to be found only within the boundary layers. The influence of the secondary motion can be detected at θ = 60° and, at the exit, the turbulence is anisotropic with high $\tilde{v}$ near the pressure surface and high $\tilde{u}$ near the suction surface. At X_H = 2.50 the behaviour of $\overline{uv}$ is complex with a large area on the suction surface being occupied by positive values of - $\overline{uv}$ and near zero values on the pressure side. Momentum transfer in the span (z^*) direction is accomplished through $\overline{uw}$, which is plotted in figure 20. Values are large near z^* = 0.5, as could be expected, because of the region of large

8

streamwise-velocity gradients present. The maximum values of $\overline{uv}$ and $\overline{uw}$ are similar $(0.003V_c^2)$ although present in different regions. The contours of $\tilde{u}$ and $\tilde{v}$ also show large changes, with maximum values of the order of 0.11 V_c. Figure 21 shows contours of the $\tilde{w}$ component of fluctuating velocity. The contours of turbulent kinetic energy were constructed from $\tilde{u}$, $\tilde{v}$ and $\tilde{w}$ measurements and are presented in figure 22.

The results from which the figures have been plotted are tabulated in Appendix 1 as Table II for the velocity measurements and Table III for the wall pressure measurements.

4. DISCUSSION

Comparison of the laminar and turbulent results shows that the influence of the bend results in a greater asymmetry about the mean radius in the upstream supply duct for turbulent flow and is associated with the favourable pressure gradient on the suction side. In contrast, the laminar flow with thicker boundary layers is found to develop larger gapwise velocities more rapidly, and over a larger region, which counteract the effect of the pressure gradient and result in smaller asymmetry at inlet. This mechanism is also evident in the fully-developed turbulent flow of reference 8 where the inlet asymmetry is smaller than in the present turbulent flow.

Within the bend the locii of the maximum streamwise velocities in figures 7 and 12 are quite different, as a consequence of the secondary flow development. The larger secondary flow in the laminar case is associated with a greater pressure loss in the bend, e.g. $0.4\rho V_c^2$ calculated in reference 7, as compared with $0.1\rho V_c^2$ for the present turbulent case.

The influence of the boundary layer thickness at the inlet can be assessed by reference to references 7 and 8. In the case of laminar flow, the maximum streamwise velocity at $\theta = 60^o$ is larger and the deceleration of fluid near the suction surface at the exit is more extensive for fully-developed boundary layers at the inlet to the bend. These differences probably reflect a more extensive streamwise vorticity with the thicker inlet boundary layer, although the locii of maximum streamwise velocity, for example, are similar. In the case of turbulent flow with fully-developed boundary layers, the profiles at the inlet are affected by secondary flows of the "second kind" driven by normal stresses which, in turn, influence the development of flow in the bend. There is no correspond-

9

ing effect in the present flow. The presence of an extensive irrotational flow at the inlet in the present data results in the first 30° behaving in a manner consistent with a potential irrotational flow with the streamwise velocity maximum occurring close to the suction surface and there is little evidence of the effect of secondary flow until $\theta = 60^\circ$. This is in contrast to reference 8, where the effects of secondary flow are evident upon entry to the bend. Beyond this station, both reference 8 and the present results show qualitatively similar behaviour with the locii of maximum streamwise velocity occurring near the mean radius of the bend. The quantitative differences in the behaviour of the streamwise isotachs suggest differences in the streamwise vorticity. Thus, in the exit plane of the present bend, there are higher negative gapwise velocities ($-0.3\ V_c$ as opposed to $-0.15\ V_c$) and smaller velocities on the symmetry plane ($0.2\ V_c$ as opposed to $0.28\ V_c$). For the fluctuating velocities there is qualitative agreement between the two flows; for example, $-\overline{uv}$ is large near the suction surface and, at the exit of the bend, $\tilde{v}$ is large near the suction surface while $\tilde{u}$ is large near the pressure surface. Quantitive agreement is not found and is not expected. For example, at the inlet $\overline{uv}$ is up to $0.0013\ V_c^2$ in the present flow as compared to $0.004\ V_c^2$ in reference 8. At exit, the respective values are $0.003\ V_c^2$ and $0.007\ V_c^2$. The influence of streamline curvature is expected to increase turbulence levels near the suction surface and to decrease them near the pressure surface and the behaviour of $\overline{uv}$ and $\tilde{v}$ support this expectation although the behaviour of $\tilde{u}$ is anomalous. No doubt convection of fluid away from the suction surface is also influential in determining the fluctuation levels in this region.

5. CONCLUDING REMARKS

1. This experimental programme has reported in detail on the velocity and pressure distribution in a square duct of strong curvature with thin inlet boundary layers for laminar and turbulent flows.

2. Secondary flows of the first kind are present in both flows and are more pronounced in the laminar flow partly because of the thicker boundary layers. The lower magnitude of secondary flows at inlet to the bend in the turbulent case results in greater asymmetries about the mean radius. Secondary velocities of up to 0.6 and 0.4 of the bulk velocity are found in the laminar and turbulent regimes respectively.

3. The position of maximum streamwise velocity migrates, in laminar flow, from the mean radius of the bend towards the pressure surface. In turbulent flow, the migration is initially towards the suction surface and lies at the mean radius at the exit. The turbulent flow behaviour is more akin to a potential irrotational flow in the entry region.

10

4. The pressure loss across the bend is about one fifth of the velocity head in the turbulent case.

5. Comparisons have been made with laminar and turbulent flows with fully-developed boundary layers at the inlet to the duct. For the laminar flow, the differences were small and in the turbulent flow the influence of streamwise vorticity is apparent much later with the thin inlet boundary layers. The trends in the fluctuating velocities and shear stress are similar although, as expected, the levels are not comparable.

6. This report presents benchmark measurements against which the results of numerical calculation methods can be compared.

APPENDIX 1

TABULATED DATA

TABLE I. 90 DEGREE BEND OF 2.3 RADIUS RATIO AND SQUARE CROSS SECTION
LAMINAR FLOW: REYNOLDS NUMBER 790 VELOCITY MEASUREMENTS
(All velocities normalised by the bulk velocity V_c = 0.0198 m/s)

Streamwise station X_H *	Spanwise location $z/z_{\frac{1}{2}}$ **	Gapwise location $\dfrac{r-r_o}{r_i-r_o}$ ***	Streamwise velocity U/V_c	Gapwise location $\dfrac{r-r_o}{r_i-r_o}$ **	Streamwise velocity U/V_c
-0.50	0.0	0.1	0.835	0.3	1.595
	0.1		0.823		1.594
	0.2		0.826		1.584
	0.3		0.814		1.547
	0.4		0.782		1.513
	0.5		0.736		1.464
	0.6		0.673		1.289
	0.7		0.543		1.087
	0.8		0.378		0.782
	0.9		0.208		0.363
	0.0	0.5	1.641	0.7	1.632
	0.1		1.641		1.610
	0.2		1.638		1.601
	0.3		1.635		1.590
	0.4		1.607		1.550
	0.5		1.575		1.491
	0.6		1.472		1.392
	0.7		1.280		1.174
	0.8		0.969		0.888
	0.9		0.512		0.356
	0.0	0.9	0.891		
	0.1		0.866		
	0.2		0.869		
	0.3		0.826		
	0.4		0.802		
	0.5		0.761		
	0.6		0.698		
	0.7		0.667		
	0.8		0.512		
	0.9		0.279		

*   Number of hydraulic diameters upstream of bend entry plane
**   Distance from plane of symmetry normalised by the duct half-span
***   Distance from outer wall normalised by the duct gap

TABLE I.   (Cont...)

Streamwise station X_H	Spanwise location $z/z_{\frac{1}{2}}$	Gapwise location $\dfrac{r-r_o}{r_i-r_o}$	Streamwise velocity U/V_c	Gapwise velocity V/V_c	Gapwise location $\dfrac{r-r_o}{r_i-r_o}$	Streamwise velocity U/V_c	Gapwise velocity V/V_c
−0.25	0.0	0.1	0.876	0.032	0.3	1.606	0.045
	0.1		0.880	0.032		1.616	0.046
	0.2		0.863	0.019		1.604	0.052
	0.3		0.869	0.017		1.579	0.052
	0.4		0.841	0.023		1.537	0.049
	0.5		0.795	0.021		1.446	0.051
	0.6		0.729	0.017		1.315	0.056
	0.7		0.615	0.021		1.115	0.082
	0.8		0.372	–		0.813	0.066
	0.9		0.197	–		0.633	0.080
	0.0	0.5	1.693	0.053	0.7	1.631	0.058
	0.1		1.691	0.052		1.640	0.045
	0.2		1.685	0.059		1.632	0.037
	0.3		1.675	0.064		1.618	0.040
	0.4		1.645	0.072		1.586	0.065
	0.5		1.565	0.088		1.522	0.072
	0.6		1.403	0.080		1.413	0.059
	0.7		1.143	0.060		1.221	0.065
	0.8		0.815	0.076		0.922	0.050
	0.9		0.651	0.062		0.363	0.060
	0.0	0.9	0.953	−0.004			
	0.1		0.929	0.002			
	0.2		0.945	0.014			
	0.3		0.911	0.006			
	0.4		0.887	0.004			
	0.5		0.833	0.016			
	0.6		0.792	0.002			
	0.7		0.693	0.008			
	0.8		0.542	−0.015			
	0.9		0.233	−0.007			

TABLE I   (Cont...)

Streamwise station θ * (deg.)	Spanwise location $z/z_{1/2}$	Gapwise location $\dfrac{r-r_o}{r_i-r_o}$	Streamwise velocity U/V_c	Gapwise velocity V/V_c	Gapwise location $\dfrac{r-r_o}{r_i-r_o}$	Streamwise velocity U/V_c	Gapwise velocity V/V_c
30	0.0	0.1	1.048	-0.116	0.3	1.624	-0.292
	0.1		1.067	-0.114		1.577	-0.294
	0.2		1.085	-0.122		1.564	-0.303
	0.3		1.078	-0.107		1.558	-0.309
	0.4		1.052	-0.093		1.558	-0.301
	0.5		1.021	-0.072		1.529	-0.276
	0.6		0.916	-0.028		1.437	-0.197
	0.7		0.786	0.052		1.248	-0.034
	0.8		0.522	0.161		0.863	0.261
	0.9		0.216	0.028		0.452	0.219
	0.0	0.5	1.708	-0.410	0.7	1.558	-0.367
	0.1		1.718	-0.408		1.552	-0.369
	0.2		1.696	-0.390		1.540	-0.358
	0.3		1.676	-0.371		1.518	-0.349
	0.4		1.632	-0.331		1.481	-0.325
	0.5		1.562	-0.261		1.419	-0.268
	0.6		1.450	-0.153		1.300	-0.127
	0.7		1.232	0.059		1.109	0.107
	0.8		0.851	0.357		0.766	0.397
	0.9		0.469	0.276		0.546	0.274
	0.0	0.9	0.722	-0.098			
	0.1		0.707	-0.096			
	0.2		0.698	-0.105			
	0.3		0.664	-0.127			
	0.4		0.667	-0.122			
	0.5		0.742	-0.114			
	0.6		0.790	-0.039			
	0.7		0.729	0.092			
	0.8		0.562	0.180			
	0.9		0.344	0.160			

* Angular position from bend entry plane

14

TABLE I   (Cont...)

Streamwise station θ (deg.)	Spanwise location z/z_1	Gapwise location $\dfrac{r-r_o}{r_i-r_o}$	Streamwise velocity U/V_c	Gapwise velocity V/V_c	Gapwise location $\dfrac{r-r_o}{r_i-r_o}$	Streamwise velocity U/V_c	Gapwise velocity V/V_c
60	0.0	0.1	1.439	-0.054	0.3	1.588	-0.287
	0.1		1.434	-0.068		1.579	-0.265
	0.2		1.439	-0.068		1.588	-0.248
	0.3		1.441	-0.070		1.569	-0.232
	0.4		1.419	-0.065		1.536	-0.182
	0.5		1.399	-0.063		1.551	-0.153
	0.6		1.351	-0.032		1.542	-0.101
	0.7		1.287	-0.004		1.491	0.020
	0.8		1.087	0.072		1.399	0.195
	0.9		0.678	0.129		1.021	0.296
	0.0	0.5	1.173	-0.259	0.7	0.580	-0.211
	0.1		1.177	-0.254		0.571	-0.231
	0.2		1.155	-0.236		0.648	-0.308
	0.3		1.123	-0.218		0.773	-0.293
	0.4		1.183	-0.186		0.926	-0.224
	0.5		1.240	-0.194		1.038	-0.117
	0.6		1.344	-0.123		1.129	0.021
	0.7		1.394	0.046		1.181	0.217
	0.8		1.338	0.153		1.236	0.541
	0.9		0.926	0.505		0.929	0.617
	0.0	0.9	0.332	-0.025			
	0.1		0.362	-0.054			
	0.2		0.469	-0.128			
	0.3		0.618	-0.176			
	0.4		0.712	-0.148			
	0.5		0.723	-0.082			
	0.6		0.748	0.074			
	0.7		0.708	0.203			
	0.8		0.530	0.199			
	0.9		0.301	0.084			

TABLE I   (Cont...)

Streamwise station θ (deg.)	Spanwise location z/z_1	Gapwise location $\dfrac{r-r_o}{r_i-r_o}$	Streamwise velocity U/V_c	Gapwise velocity V/V_c	Gapwise location $\dfrac{r-r_o}{r_i-r_o}$	Streamwise velocity U/V_c	Gapwise velocity V/V_c
77.5	0.0	0.1	1.553	-0.041	0.3	1.533	-0.136
	0.1		1.555	-0.043		1.542	-0.136
	0.2		1.542	-0.057		1.545	-0.133
	0.3		1.549	-0.054		1.549	-0.129
	0.4		1.533	-0.048		1.571	-0.133
	0.5		1.512	-0.039		1.595	-0.127
	0.6		1.468	-0.026		1.632	-0.107
	0.7		1.390	-0.015		1.652	-0.030
	0.8		1.210	0.046		1.565	0.131
	0.9		0.802	0.133		1.095	0.354
	0.0	0.5	0.735	-0.072	0.7	0.562	-0.052
	0.1		0.745	-0.063		0.614	-0.114
	0.2		0.782	-0.096		0.685	-0.224
	0.3		0.823	-0.098		0.760	-0.255
	0.4		0.955	-0.142		0.921	-0.209
	0.5		1.087	-0.164		0.951	-0.024
	0.6		1.281	-0.191		0.944	0.127
	0.7		1.507	-0.162		1.044	0.176
	0.8		1.463	0.153		1.300	0.237
	0.9		0.986	0.322		0.845	0.358
	0.0	0.9	0.369	-0.009			
	0.1		0.326	-0.024			
	0.2		0.294	-0.092			
	0.3		0.505	-0.215			
	0.4		0.920	-0.248			
	0.5		1.169	-0.105			
	0.6		1.245	0.068			
	0.7		1.232	0.204			
	0.8		1.028	0.289			
	0.9		0.503	0.160			

TABLE I   (Cont...)

Streamwise station $X_H{}^*$	Spanwise location $z/z_{\frac{1}{2}}$	Gapwise location $\dfrac{r-r_o}{r_i-r_o}$	Streamwise velocity U/V_c	Gapwise velocity V/V_c	Gapwise location $\dfrac{r-r_o}{r_i-r_o}$	Streamwise velocity U/V_c	Gapwise velocity V/V_c
+0.25	0.0	0.1	1.711	-0.028	0.3	1.471	-0.053
	0.1		1.712	-0.029		1.476	-0.082
	0.2		1.711	-0.028		1.487	-0.076
	0.3		1.716	-0.028		1.5o1	-0.089
	0.4		1.718	-0.039		1.511	-0.114
	0.5		1.716	-0.041		1.544	-0.138
	0.6		1.694	-0.032		1.621	-0.154
	0.7		1.661	-0.008		1.693	-0.082
	0.8		1.523	0.028		1.650	0.081
	0.9		1.093	0.130		1.156	0.224
	0.0	0.5	0.772	0.014	0.7	0.550	-0.016
	0.1		0.773	0.000		0.539	-0.055
	0.2		0.762	-0.024		0.681	-0.171
	0.3		0.761	-0.058		0.943	-0.251
	0.4		0.790	-0.061		1.061	-0.191
	0.5		0.852	-0.052		1.032	-0.013
	0.6		1.037	-0.074		0.969	0.112
	0.7		1.300	-0.092		1.083	0.122
	0.8		1.278	0.087		1.131	0.142
	0.9		0.831	0.185		0.687	0.141
	0.0	0.9	0.311	-0.017			
	0.1		0.331	-0.065			
	0.2		0.484	-0.113			
	0.3		0.782	-0.151			
	0.4		1.034	-0.107			
	0.5		1.126	-0.031			
	0.6		1.148	0.028			
	0.7		1.078	0.085			
	0.8		0.780	0.094			
	0.9		0.382	0.070			

*Number of hydraulic diameters downstream of bend exit plane.

TABLE I (Cont...)

Streamwise station X_H	Spanwise location $z/z_{1/2}$	Gapwise location $\dfrac{r-r_o}{r_i-r_o}$	Streamwise velocity U/V_c		Gapwise location $\dfrac{r-r_o}{r_i-r_o}$	Streamwise velocity U/V_c
+0.40	0.0	0.1	1.704		0.3	1.497
	0.1		1.706			1.523
	0.2		1.706			1.520
	0.3		1.713			1.513
	0.4		1.707			1.523
	0.5		1.709			1.547
	0.6		1.698			1.587
	0.7		1.698			1.669
	0.8		1.580			1.656
	0.9		1.109			1.131
	0.0	0.5	0.794		0.7	0.519
	0.1		0.754			0.577
	0.2		0.736			0.782
	0.3		0.733			0.984
	0.4		0.767			1.062
	0.5		0.811			1.025
	0.6		0.990			0.984
	0.7		1.308			1.124
	0.8		1.345			1.119
	0.9		0.674			0.588
	0.0	0.9	0.272			
	0.1		0.279			
	0.2		0.379			
	0.3		0.624			
	0.4		0.882			
	0.5		1.049			
	0.6		1.096			
	0.7		1.096			
	0.8		0.770			
	0.9		0.365			

TABLE I (Cont...)

Streamwise station X_H	Spanwise location $z/z_{\frac{1}{2}}*$	Gapwise location $\dfrac{r-r_o}{r_i-r_o}$	Streamwise velocity U/V_c	Gapwise velocity V/V_c $\times 10^2$	Spanwise velocity W/V_c $\times 10^2$
+2.50	0.0	0.1	1.393	0.000	0.000
	0.1		1.393	0.000	0.000
	0.2		1.403	0.000	0.000
	0.3		1.403	0.000	1.397
	0.4		1.403	1.397	1.397
	0.5		1.403	1.397	2.795
	0.6		1.383	1.397	2.069
	0.7		1.334	1.397	1.397
	0.8		1.166	1.397	0.000
	0.9		0.790	1.397	0.000
	0.0	0.3	1.512	4.193	0.000
	0.1		1.512	4.193	0.000
	0.2		1.512	2.795	0.000
	0.3		1.502	0.000	0.000
	0.4		1.482	-4.193	0.000
	0.5		1.423	-4.892	0.000
	0.6		1.482	-4.193	0.000
	0.7		1.581	1.397	1.398
	0.8		1.581	4.193	1.398
	0.9		1.186	0.000	2.796

19

TABLE I (Cont...)

Streamwise station X_H	Spanwise location $z/z_{\frac{1}{2}}$	Gapwise location $\dfrac{r-r_o}{r_i-r_o}$	Streamwise velocity U/V_c	Gapwise velocity V/V_c $\times 10^2$	Spanwise velocity W/V_c $\times 10^2$
+2.50	0.0	0.5	1.091	0.139	0.699
	0.1		1.043	-0.139	3.709
	0.2		0.984	-0.978	5.730
	0.3		0.931	-3.075	6.710
	0.4		0.919	-2.796	6.570
	0.5		0.946	-3.215	5.172
	0.6		1.045	-1.677	3.355
	0.7		1.170	1.677	1.118
	0.8		1.027	1.957	0.139
	0.9		0.575	0.838	0.559
	0.0	0.7	0.812	-11.743	-0.414
	0.1		0.871	-12.023	-2.935
	0.2		0.992	-10.765	-2.376
	0.3		1.075	-8.668	-2.239
	0.4		1.055	-4.194	-0.978
	0.5		1.034	1.258	-1.398
	0.6		1.029	5.732	-1.817
	0.7		1.023	8.108	-2.234
	0.8		0.879	6.291	-1.537
	0.85		-	-	-0.838
	0.9		0.512	2.376	
	0.0	0.9	0.482	-2.516	0.265
	0.1		0.543	-2.655	-0.419
	0.2		0.662	-3.075	-2.656
	0.3		0.763	-2.655	-5.732
	0.4		0.816	-1.258	-7.269
	0.5		0.820	0.559	-6.990
	0.6		0.765	1.817	-6.291
	0.7		0.652	1.957	-3.215
	0.80		0.470	0.838	-1.398
	0.85		-	-	-0.559
	0.90		0.251	0.276	-

Table II.   90 DEGREE BEND OF 2.3 RADIUS RATIO AND SQUARE CROSS-SECTION
TURBULENT FLOW: MEAN VELOCITY, TURBULENCE LEVEL AND CROSS-
CORRELATION MEASUREMENTS, REYNOLDS NUMBER 40 000
(All quantities normalised by bulk velocity V_c= 1.002 m/s)

Streamwise station X_H*	Spanwise location $z/z_{\frac{1}{2}}$**	Gapwise location $\dfrac{r-r_o}{r_i-r_o}$***	Streamwise mean veloc $\bar{u}/V_c$	Streamwise turb. level $\tilde{u}/V_c$ x10^2	Gapwise mean veloc $\bar{V}/V_c$ x10^2	Gapwise turb. level $\tilde{v}/V_c$ x10^2	Cross correlation $-\overline{uv}/V_c^2$ x10^3
-0.25	0.0	0.1	0.931	6.546	2.762	4.086	1.181
	0.1		0.929	6.485	2.762	4.200	1.181
	0.2		0.933	6.423	2.762	4.076	1.102
	0.3		0.929	6.546	2.485	4.134	1.128
	0.4		0.914	6.794	2.485	3.923	1.128
	0.5		0.914	6.794	2.485	3.701	1.208
	0.6		0.910	6.794	2.485	4.127	1.290
	0.7		0.906	6.794	1.933	4.430	0.918
	0.8		0.847	6.917	1.933	4.931	-0.292
	0.9		0.691	9.511	1.933	5.553	-0.280
	0.915		0.632	9.765	1.933	4.559	-0.297
	0.930		0.535	11.328	1.657	3.084	-0.640
	0.950		0.496	12.109	1.381	—	—
	0.0	0.3	1.085	0.781	4.695	1.002	0.014
	0.1		1.082	0.781	4.695	0.989	0.008
	0.2		1.082	0.781	4.695	1.105	0.207
	0.3		1.082	0.781	4.695	1.120	0.003
	0.4		1.082	0.898	4.695	1.358	0.000
	0.5		1.082	1.132	4.143	2.009	0.009
	0.6		1.070	2.773	4.143	3.599	0.000
	0.7		1.007	5.558	4.143	4.916	0.088
	0.8		0.902	7.535	4.419	5.975	0.153
	0.9		0.738	9.882	4.143	6.047	0.099
	0.915		0.695	10.499	4.419	5.608	-0.742
	0.930		0.625	11.328	3.314	4.538	-1.716
	0.950		0.515	12.500	2.009	—	—

*   Number of hydraulic diameters upstream of bend entry plane
**   Distance from plane of symmetry normalised by the duct half-span
***   Distance from outer wall normalised by the duct gap.

TABLE II. (Cont....)

Streamwise station X_H	Spanwise location z/z_1	Gapwise location $\dfrac{r-r_o}{r_i-r_o}$	Streamwise mean velocity $\bar{U}/V_c$	Streamwise turb. level $\tilde{u}/V_c \times 10^2$	Gapwise mean velocity $\bar{V}/V_c$	Gapwise turb. level $\tilde{v}/V_c \times 10^2$	cross correlation $-\overline{uv}/V_c^2 \times 10^3$
-0.25	0.0	0.5	1.109	0.742	4.695	0.385	-0.002
	0.1		1.105	0.742	4.695	0.536	-0.002
	0.2		1.105	0.742	4.695	0.591	-0.007
	0.3		1.105	0.742	4.695	0.810	-0.002
	0.4		1.105	0.742	4.975	0.893	-0.040
	0.5		1.101	1.230	4.975	1.312	-0.015
	0.6		1.074	3.125	4.975	2.854	0.046
	0.7		1.019	5.126	4.975	4.456	0.293
	0.8		0.914	7.164	4.975	5.018	0.305
	0.9		0.753	9.635	5.524	6.214	0.098
	0.915		0.718	10.438	4.419	6.413	0.102
	0.930		0.640	12.109	3.869	6.861	-1.305
	0.950		0.542	13.281	3.033	.-	-
	0.0	0.7	1.134	0.781	4.419	0.896	-0.006
	0.1		1.128	0.781	4.419	0.930	-0.003
	0.2		1.128	0.781	4.419	0.930	-0.003
	0.3		1.128	0.820	4.143	1.009	-0.036
	0.4		1.128	0.859	4.419	1.015	-0.014
	0.5		1.128	1.250	4.419	1.005	-0.008
	0.6		1.117	2.343	4.419	2.068	-0.008
	0.7		1.070	4.690	4.419	3.211	-0.148
	0.8		0.968	6.794	4.419	5.079	-0.222
	0.9		0.812	8.955	4.419	6.044	-0.037
	0.915		0.750	10.499	4.419	6.302	-0.903
	0.930		0.667	12.402	3.314	3.894	-0.701
	0.950		0.578	13.281	2.485	-	-
	0.0	0.9	1.035	5.682	3.038	3.900	-0.995
	0.1		1.035	5.929	3.038	3.837	-1.024
	0.2		1.040	5.929	3.038	3.713	-1.071
	0.3		1.035	5.929	3.038	3.837	-1.281
	0.4		1.031	6.546	3.038	3.960	-1.281
	0.5		1.027	6.299	3.038	4.232	-1.409
	0.6		1.027	5.805	3.314	4.262	-1.024
	0.7		1.015	5.805	3.590	4.332	-0.803
	0.8		0.933	6.917	3.038	5.229	-0.528
	0.9		0.789	9.264	0.552	5.963	-0.476
	0.915		0.734	10.561	0.552	6.148	-1.055
	0.930		0.628	12.109	0.276	4.690	-
	0.950		0.558	13.281	0.276	.-	-

TABLE II (cont...)

Streamwise station θ* (deg.)	Spanwise location z/z_l	Gapwise location $\dfrac{r-r_o}{r_i-r_o}$	Streamwise velocity $\bar{U}/V_c$	Streamwise turbulence level $\tilde{u}/V_c$ $\times10^2$	Gapwise velocity $\bar{V}/V_c$ $\times10^2$	Gapwise turbulence level $\tilde{v}/V_c$ $\times10^2$	Cross correlation $-\overline{uv}/V_c^2$ $\times10^3$
30	0.0	0.1	0.789	8.984	-3.314	7.572	4.696
	0.1		0.789	8.882	-4.419	7.264	4.568
	0.2		0.789	8.984	-4.971	6.665	4.421
	0.3		0.785	9.375	-4.143	7.222	4.635
	0.4		0.777	9.635	-2.485	7.585	4.635
	0.5		0.757	10.499	-1.657	7.559	4.730
	0.6		0.750	10.546	-1.381	7.480	5.371
	0.7		0.746	10.623	-1.381	7.125	4.223
	0.8		0.710	9.765	-0.276	6.622	3.543
	0.9		0.660	9.388	1.657	5.931	2.667
	0.915		0.609	8.984	4.971	5.449	2.307
	0.930		0.546	9.765	6.352	5.290	2.260
	0.950		0.480	11.328	7.181	-	0.984
	0.0	0.3	1.062	1.210	-5.800	1.560	0.048
	0.1		1.058	1.457	-5.690	1.605	0.048
	0.2		1.058	1.484	-5.800	1.610	0.050
	0.3		1.058	1.523	-6.076	1.579	0.060
	0.4		1.058	1.562	-6.284	1.450	0.060
	0.5		1.062	1.601	-6.905	1.826	0.051
	0.6		1.055	1.992	-7.098	2.657	0.085
	0.7		1.030	3.495	-5.521	3.656	0.205
	0.8		0.963	5.682	0.550	5.958	0.496
	0.9		0.856	8.245	12.291	7.449	0.295
	0.0	0.5	1.142	0.703	-8.015	0.605	-0.028
	0.1		1.148	0.781	-8.015	0.615	-0.028
	0.2		1.148	0.820	-8.563	0.610	-0.028
	0.3		1.148	0.859	-8.832	0.610	-0.028
	0.4		1.148	0.976	-9.391	0.629	-0.064
	0.5		1.152	1.093	-9.667	1.222	-0.027
	0.6		1.142	2.265	-9.501	2.591	0.061
	0.7		1.109	4.076	-6.465	4.115	0.460
	0.8		1.022	6.917	3.972	5.956	2.024
	0.9		0.871	10.005	14.250	6.285	1.900

*Angular position from bend entry plane

23

TABLE II (Cont...)

Streamwise station θ (deg)	Spanwise location $z/z_{\frac{1}{2}}$	Gapwise location $\dfrac{r-r_o}{r_i-r_o}$	Streamwise velocity U/V_c	Streamwise turbulence level $\hat{u}/V_c$ $\times 10^2$	Gapwise velocity $\bar{V}/V_c$	Gapwise turbulence level $\hat{v}/V_c$ $\times 10^2$	Cross correlation $-\overline{uv}/V_c^2$ $\times 10^3$
30	0.0	0.7	1.257	1.093	-8.838	0.495	0.009
	0.1		1.257	0.937	-8.675	0.587	0.009
	0.2		1.257	0.976	-8.563	0.579	0.009
	0.3		1.255	0.976	-8.838	0.629	0.006
	0.4		1.253	1.054	-9.556	0.881	0.014
	0.5		1.253	1.328	-9.865	1.965	0.016
	0.6		1.231	2.594	-9.391	2.947	0.032
	0.7		1.191	4.199	-5.415	4.515	0.320
	0.8		1.121	5.929	2.563	6.049	0.732
	0.9		0.981	8.893	15.575	7.315	1.389
	0.0	0.9	1.190	4.199	-4.529	2.215	0.283
	0.1		1.191	4.199	-4.529	2.419	0.329
	0.2		1.200	3.952	-4.772	2.845	0.256
	0.3		1.200	4.076	-5.800	2.419	0.329
	0.4		1.209	4.484	-6.623	1.895	0.428
	0.5		1.209	4.570	-7.345	2.353	0.354
	0.6		1.204	4.694	-7.927	2.622	0.225
	0.7		1.178	4.817	-5.800	3.386	0.403
	0.8		1.117	6.423	-1.653	3.584	0.732
	0.9		1.018	8.152	8.479	4.710	1.132

TABLE II. (Cont...)

Streamwise station θ (deg.)	Spanwise location $z/z_{\frac{1}{2}}$	Gapwise location $\dfrac{r-r_o}{r_i-r_o}$	Streamwise mean veloc $\bar{u}/V_c$	Streamwise turb. level $\tilde{u}/V_c$ $\times 10^2$	Gapwise mean veloc $\bar{V}/V_c$ $\times 10^2$	Gapwise turb. level $\tilde{v}/V_c$ $\times 10^2$	Cross correlation $-\overline{uv}/V_c^2$ $\times 10^3$
60	0.0	0.1	0.839	8.770	-3.590	8.011	3.967
	0.1		0.839	8.646	-4.695	8.268	3.967
	0.2		0.835	8.523	-5.248	7.782	3.972
	0.3		0.832	8.646	-5.248	7.675	3.972
	0.4		0.812	8.770	-5.248	8.046	3.710
	0.5		0.800	8.893	-3.314	9.147	3.972
	0.6		0.796	9.264	-1.795	9.179	4.272
	0.7		0.792	9.388	-1.519	9.073	4.272
	0.8		0.781	9.264	-0.828	8.997	4.272
	0.9		0.742	9.017	1.657	8.566	3.158
	0.915		0.730	9.017	2.209	8.566	2.777
	0.930		0.671	9.246	2.209	8.275	1.922
	0.950		0.625	9.511	5.248	-	1.538
	0.0	0.3	1.068	2.539	-5.109	5.396	1.081
	0.1		1.064	2.737	-5.109	5.347	1.073
	0.2		1.064	2.773	-4.695	5.320	1.300
	0.3		1.064	2.773	-4.907	5.339	1.175
	0.4		1.071	2.656	-4.613	5.196	0.851
	0.5		1.066	2.964	-4.613	5.233	0.906
	0.6		1.063	3.458	-4.613	4.932	1.007
	0.7		1.062	3.582	-4.221	4.853	1.020
	0.8		1.036	4.570	-0.825	5.365	1.089
	0.9		0.927	8.593	8.700	6.571	2.047
	0.915		0.832	9.758	13.810	8.147	3.946
	0.930		0.816	10.252	14.363	7.860	3.735
	0.950		0.785	10.746	18.230	-	3.618
	0.0	0.5	1.167	0.859	-11.062	0.945	0.044
	0.1		1.167	0.871	-10.705	0.945	0.044
	0.2		1.167	0.898	-10.705	0.956	0.103
	0.3		1.167	0.898	-10.106	1.125	0.000
	0.4		1.167	1.093	-9.805	1.270	-0.023
	0.5		1.167	1.390	-9.942	1.400	-0.023
	0.6		1.164	2.420	-8.427	1.526	-0.011
	0.7		1.154	3.211	-4.883	3.786	-0.034
	0.8		1.105	5.435	4.615	6.947	-0.076
	0.9		1.007	8.276	19.770	7.912	-0.396
	0.915		0.941	8.276	28.173	8.315	1.927
	0.930		0.914	8.893	32.040	8.542	2.651
	0.950		0.871	10.252	32.593	6.916	1.398

TABLE II. (Cont...)

Streamwise station θ (deg.)	Spanwise location $z/z_{\frac{1}{2}}$	Gapwise location $\dfrac{r-r_o}{r_i-r_o}$	Streamwise mean veloc $\bar{u}/v_c$	Streamwise turb. level $\tilde{u}/v_c$ x10^2	Gapwise mean veloc $\bar{v}/v_c$ x10^2	Gapwise turb. level $\tilde{v}/v_c$ x10^2	Cross-relation $-\overline{uv}/v_c^2$ x10^3
60	0.0	0.7	1.222	2.121	-14.473	3.110	0.269
	0.1		1.222	2.148	-13.251	3.000	0.219
	0.2		1.226	2.226	-13.589	3.056	0.219
	0.3		1.226	2.210	-14.599	2.948	0.205
	0.4		1.230	2.460	-15.907	2.977	0.134
	0.5		1.226	2.773	-15.213	2.795	0.102
	0.6		1.230	3.891	-10.604	3.806	0.300
	0.7		1.200	4.694	-2.095	6.205	0.695
	0.8		1.180	6.546	12.213	7.739	1.625
	0.9		1.085	8.646	32.915	8.698	2.081
	0.915		0.968	8.770	37.845	9.256	1.880
	0.930		0.949	9.017	41.432	8.766	1.855
	0.950		0.917	9.635	43.641	7.872	1.300
	0.0	0.9	1.053	3.231	-13.905	3.579	-0.058
	0.1		1.035	4.205	-14.512	3.731	-0.324
	0.2		0.962	7.089	-21.075	4.052	-2.195
	0.3		0.968	6.085	-15.625	3.976	-1.175
	0.4		1.040	5.313	-9.667	3.886	-0.402
	0.5		1.097	3.660	-9.110	5.150	-0.140
	0.6		1.128	4.362	-4.782	6.203	0.000
	0.7		1.164	4.761	1.182	7.158	0.230
	0.8		1.164	8.357	12.805	7.631	0.720
	0.9		1.097	9.570	29.102	8.509	0.750
	0.915		0.949	10.376	36.183	9.718	1.977
	0.930		0.906	10.546	38.669	8.493	0.373
	0.950		0.847	12.109	38.669	-	-3.417

26

TABLE II (Cont...)

Streamwise station θ (deg.)	Spanwise location $z/z_{1/2}$	Gapwise location $\dfrac{r-r_o}{r_i-r_o}$	Streamwise velocity $\overline{U}/V_c$	Streamwise turbulence level u/V_c $\times 10^2$	Gapwise velocity $\overline{v}/V_c$ $\times 10^2$	Gapwise turbulence level v/V_c $\times 10^2$	Cross correlation $-\overline{uv}/V_c^2$ $\times 10^3$
77.5	0.0	0.1	0.871	7.782	-2.485	8.378	4.035
	0.1		0.867	7.782	-2.209	8.683	3.710
	0.2		0.867	7.905	-2.485	8.683	3.710
	0.3		0.867	7.782	-2.485	9.091	3.348
	0.4		0.867	7.782	-2.762	9.091	3.348
	0.5		0.859	8.029	-3.038	8.445	2.854
	0.6		0.859	8.029	-3.038	8.306	2.854
	0.7		0.859	8.029	-0.828	7.963	2.883
	0.8		0.835	8.029	-0.276	8.050	2.114
	0.9		0.789	8.152	3.314	8.090	1.983
	0.915		0.777	7.905	3.590	8.740	1.635
	0.930		0.753	8.152	3.638	8.590	1.338
	0.950		0.730	8.770	5.524	8.540	0.854
	0.0	0.3	1.066	2.506	-9.521	4.261	0.135
	0.1		1.066	3.166	-8.502	4.336	0.336
	0.2		1.064	3.875	-7.599	4.502	0.508
	0.3		1.054	4.282	-6.739	4.762	1.165
	0.4		1.046	5.473	-5.635	5.438	1.798
	0.5		1.030	5.747	-4.804	6.716	2.636
	0.6		1.027	5.921	-4.972	6.903	3.187
	0.7		1.023	6.172	-3.310	8.583	3.605
	0.8		1.027	6.429	1.933	8.936	3.830
	0.9		0.972	8.125	9.115	9.598	3.938
	0.915		0.871	9.388	12.153	9.798	3.710
	0.930		0.835	10.005	11.600	9.275	3.055
	0.950		0.816	10.252	11.877	–	2.114

TABLE II (Cont...)

Streamwise station θ (deg)	Spanwise location $z/z_{\frac{1}{2}}$	Gapwise location $\dfrac{r-r_o}{r_i-r_o}$	Streamwise velocity $\overline{U}/V_c$	Streamwise turbulence level $\tilde{u}/V_c$ $\times 10^2$	Gapwise velocity $\overline{V}/V_c$ $\times 10^2$	Gapwise turbulence level $\acute{v}/V_c$ $\times 10^2$	Cross correlation $-\overline{uv}/V_c^2$ $\times 10^3$
77.5	0.0	0.5	1.179	1.042	-15.705	1.935	-0.066
	0.1		1.180	1.054	-14.993	1.935	-0.066
	0.2		1.183	1.132	-14.206	2.057	-0.029
	0.3		1.183	1.171	-13.863	2.060	-0.048
	0.4		1.183	1.250	-13.321	2.117	-0.063
	0.5		1.185	1.367	-12.915	2.495	-0.093
	0.6		1.179	1.835	-11.019	2.668	-0.053
	0.7		1.167	2.968	-8.284	3.410	0.467
	0.8		1.144	4.941	1.672	6.170	0.686
	0.9		1.078	7.411	14.317	7.015	1.248
	0.0	0.7	1.093	3.333	-23.101	3.094	-0.038
	0.1		1.102	3.210	-22.316	3.094	-0.034
	0.2		1.121	3.397	-20.927	2.915	-0.038
	0.3		1.135	3.520	-19.162	2.697	-0.019
	0.4		1.147	3.582	-17.825	2.976	-0.065
	0.5		1.165	3.952	-16.721	3.073	0.190
	0.6		1.187	4.696	-12.503	3.593	0.195
	0.7		1.213	5.929	-4.884	4.645	0.272
	0.8		1.204	7.411	9.110	7.949	0.945
	0.9		1.121	8.399	25.334	11.423	0.987
	0.0	0.9	0.661	8.314	-5.802	4.466	0.165
	0.1		0.669	10.427	-8.596	4.845	-0.195
	0.2		0.792	10.615	-16.486	6.471	-0.804
	0.3		0.936	7.605	-17.602	6.710	-0.530
	0.4		1.007	7.163	-12.711	6.259	-0.263
	0.5		1.079	6.956	-7.015	5.710	0.235
	0.6		1.139	7.231	-2.671	5.752	0.611
	0.7		1.170	7.853	4.149	6.827	1.296
	0.8		1.164	8.525	13.119	8.339	1.725
	0.9		1.053	10.405	20.407	9.933	0.000

TABLE II (Cont...)

Streamwise station X_H *	Spanwise location $z/z_{1/2}$	Gapwise location $\dfrac{r-r_o}{r_i-r_o}$	Streamwise velocity $\bar{U}/V_c$	Streamwise turbulence level $\tilde{u}/V_c$ x10^2	Gapwise velocity $\bar{V}/V_c$	Gapwise turbulence level $\tilde{v}/V_c$ x10^2	Cross correlation $-\overline{uv}/V_c^2$ x10^3
+0.25	0.0	0.1	1.035	6.176	-2.761	7.398	2.204
	0.1		1.035	6.176	-3.590	7.398	2.204
	0.2		1.035	6.299	-3.866	7.398	2.204
	0.3		1.031	6.917	-2.485	7.931	2.588
	0.4		1.031	6.917	-1.657	8.325	3.422
	0.5		1.031	6.546	-1.104	8.256	2.465
	0.6		1.031	6.546	-1.381	7.661	2.392
	0.7		1.019	6.670	-0.828	7.687	2.087
	0.8		1.007	6.670	1.104	7.550	1.565
	0.9		0.984	6.670	4.281	8.379	1.116
	0.915		0.976	6.794	6.067	8.293	1.303
	0.930		0.960	6.917	6.352	7.798	0.817
	0.950		0.949	7.288	6.629	–	0.567
	0.0	0.3	1.144	4.362	-12.306	6.345	1.182
	0.1		1.142	4.974	-11.510	6.655	1.338
	0.2		1.136	5.560	-9.805	7.316	1.160
	0.3		1.125	6.055	-6.629	9.562	1.285
	0.4		1.111	6.912	-3.507	9.173	2.728
	0.5		1.109	7.113	-2.872	8.459	3.187
	0.6		1.094	7.205	-2.486	8.015	3.000
	0.7		1.084	7.165	-1.104	7.561	2.472
	0.8		1.083	7.288	1.858	7.298	1.943
	0.9		1.054	8.072	5.882	6.770	1.742
	0.915		0.980	8.770	11.324	9.356	2.541
	0.930		0.964	–	11.048	10.507	2.453
	0.950		0.953	–	10.772	–	1.460
	0.0	0.5	1.140	3.333	-17.133	3.157	-0.226
	0.1		1.148	3.165	-16.814	3.093	-0.305
	0.2		1.165	3.030	-16.297	3.217	-0.305
	0.3		1.165	2.751	-15.178	3.562	-0.322
	0.4		1.173	2.660	-13.816	3.603	-0.395
	0.5		1.175	2.473	-10.510	3.679	-0.077
	0.6		1.175	2.595	-8.752	3.945	0.000
	0.7		1.179	2.914	-6.903	4.421	0.165
	0.8		1.178	4.321	2.845	5.893	1.142
	0.9		1.113	7.421	14.106	8.667	2.656
	0.915		1.062	7.575	16.572	7.923	2.902
	0.930		1.023	8.593	17.401	7.629	2.195
	0.950		0.980	9.765	22.649	–	–

* Number of hydraulic diameters downstream of bend exit plane

29

TABLE II (Cont...)

Streamwise station X_H	Spanwise location $z/z_{\frac{1}{2}}$	Gapwise location $\dfrac{r-r_o}{r_i-r_o}$	Streamwise velocity $\overline{U}/V_c$	Streamwise turbulence level u/V_c $\times 10^2$	Gapwise velocity $\overline{V}/V_c$ $\times 10^2$	Gapwise turbulence level v'/V_c $\times 10^2$	Cross correlation $-\overline{uv}/V_c$ $\times 10^3$
+0.25	0.0	0.7	0.601	7.416	-18.915	4.943	1.523
	0.1		0.636	7.537	-18.236	5.728	1.396
	0.2		0.695	7.575	-15.318	6.587	1.226
	0.3		0.753	7.906	-8.126	5.523	0.415
	0.4		0.882	7.943	-2.485	5.256	0.249
	0.5		0.978	5.103	-6.542	4.845	-0.349
	0.6		1.040	4.321	-5.083	4.852	-0.490
	0.7		1.096	5.103	-1.570	5.102	-0.217
	0.8		1.152	6.210	6.435	6.067	-0.265
	0.9		1.131	7.031	18.782	7.509	1.739
	0.915		1.082	7.657	26.240	8.596	1.222
	0.930		1.039	8.593	28.450	8.245	0.984
	0.950		1.007	9.375	29.002	–	0.000
	0.0	0.9	.0.506	8.962	-4.615	3.388	-0.020
	0.1		0.500	10.107	-5.973	3.825	0.521
	0.2		0.617	13.730	-12.198	4.156	3.158
	0.3		0.830	12.226	-10.219	4.492	2.157
	0.4		0.971	8.159	-10.493	4.763	0.329
	0.5		1.035	7.166	-6.241	5.928	-0.808
	0.6		1.070	6.862	1.108	6.785	-1.205
	0.7		1.093	7.043	8.283	7.477	0.403
	0.8		1.089	7.537	12.291	5.455	0.985
	0.9		1.019	8.593	16.744	4.353	-0.142
	0.915		0.996	9.015	28.173	9.061	-0.276
	0.930		0.941	10.546	30.935	8.939	-0.763
	0.950		0.906	12.109	27.068	–	–

TABLE II   (Cont....)

Streamwise station x_H	Spanwise location z/z_4	Gapwise location $\dfrac{r-r_o}{r_i-r_o}$	Streamwise mean veloc. $\bar{U}/V_c$ ×10²	Streamwise turb.level $\tilde{u}/V_c$ ×10²	Gapwise mean veloc. $\bar{V}/V_c$ ×10²	Gapwise turb.level $\tilde{v}/V_c$ ×10²	Spanwise mean veloc. $\bar{W}/V_c$ ×10²	Spanwise turb.level $\tilde{w}/V_c$ ×10²	Cross-correlat. $-\overline{uv}/V_c^2$ ×10³	Cross-correlat. $-\overline{uw}/V_c^2$ ×10³
+2.50	0.0	0.1	1.136	5.311	-2.485	3.663	0.000	4.963	0.549	0.000
	0.1		1.136	5.311	-2.485	4.079	0.000	5.069	0.514	0.000
	0.2		1.136	5.311	-2.485	4.200	0.690	4.809	0.463	-0.125
	0.3		1.136	5.311	-1.933	4.200	0.690	4.551	0.595	-0.244
	0.4		1.126	5.682	-1.657	4.263	3.038	5.055	0.432	-0.393
	0.5		1.117	5.929	-0.828	4.782	3.038	5.555	0.393	-0.212
	0.6		1.117	6.176	0.828	5.122	1.381	5.183	0.569	0.134
	0.7		1.117	6.176	1.381	5.479	1.381	4.639	0.638	0.137
	0.8		1.113	6.052	1.104	5.618	1.104	4.221	0.717	-0.185
	0.9		1.093	6.917	2.209	5.656	1.657	4.116	0.622	-0.324
	0.915		1.042	7.658	1.381	5.201	-	-	0.161	-
	0.930		1.007	8.893	1.104	5.212	-	-	-0.180	-
	0.950		0.953	10.993	0.828	-	-	-	-1.198	-
	0.0	0.3	1.113	9.264	-3.590	8.517	0.552	6.969	-2.368	0.127
	0.1		1.113	9.011	-3.590	8.361	2.485	6.428	-2.368	1.046
	0.2		1.125	8.276	-3.314	7.901	3.314	6.278	-2.574	1.062
	0.3		1.140	7.720	-2.485	7.912	3.869	5.781	-2.081	0.720
	0.4		1.153	6.299	-1.657	6.738	4.143	5.027	-0.881	0.347
	0.5		1.156	5.558	-1.657	5.425	4.143	4.666	-0.064	0.189
	0.6		1.164	5.188	-1.104	4.691	3.866	4.038	0.119	-0.069
	0.7		1.164	5.311	1.104	4.203	3.314	4.091	0.463	-0.320
	0.8		1.152	5.929	3.038	5.116	3.038	4.035	0.671	-0.225
	0.9		1.128	7.102	7.733	5.860	2.209	3.950	0.503	-0.503
	0.915		1.074	8.276	9.391	8.021	-	-	-0.374	-
	0.930		1.050	8.984	10.219	7.415	-	-	-0.736	-
	0.950		0.992	11.718	7.457	-	-	-	-2.191	-

TABLE II (Cont...)

Streamwise station x_H	Spanwise location z/z_b	Gapwise location $\frac{r-r_o}{r_i-r_o}$	Streamwise mean veloc. $\bar{U}/v_c$	Streamwise turb.level $\tilde{u}/v_c \times 10^2$	Gapwise mean veloc. $\bar{V}/v_c \times 10^2$	Gapwise turb.level $\tilde{v}/v_c \times 10^2$	Spanwise mean veloc. $\bar{W}/v_c \times 10^2$	Spanwise turb.level $\tilde{w}/v_c \times 10^2$	Cross-Correlat. $-\overline{uv}/v_c^2 \times 10^3$	Cross-Correlat. $-\overline{uw}/v_c^2 \times 10^3$
+2.50	0.0	0.5	0.757	9.511	-8.838	11.812	-0.138	7.530	-1.969	-0.213
	0.1		0.757	9.765	-8.286	11.750	1.657	7.972	-2.163	0.213
	0.2		0.757	10.546	-5.248	10.309	4.419	8.484	-2.830	0.110
	0.3		0.773	10.937	-0.828	9.789	6.352	8.789	-3.639	0.826
	0.4		0.808	10.937	0.276	8.358	6.352	9.106	-3.967	2.281
	0.5		0.886	12.109	2.485	7.833	5.524	9.603	-3.967	3.639
	0.6		0.980	10.546	2.762	6.869	4.695	8.725	-2.403	3.364
	0.7		1.078	7.905	5.248	5.962	4.143	7.663	-1.063	2.082
	0.8		1.125	6.423	7.457	5.662	3.038	5.948	0.150	0.457
	0.9		1.125	8.399	11.048	7.001	2.209	4.535	0.567	-0.394
	0.915		1.070	8.593	12.153	7.118	-	-	0.000	-
	0.930		1.019	9.765	11.877	7.239	-	-	0.000	-
	0.950		0.957	11.328	10.496	6.989	-	-	-1.464	-
	0.0	0.7	0.839	7.788	-23.750	7.691	0.414	9.039	0.830	-0.103
	0.1		0.849	8.029	-20.432	8.423	0.552	8.820	1.812	-0.530
	0.2		0.839	8.152	-14.910	10.127	0.828	8.654	2.896	-1.149
	0.3		0.808	8.203	-7.181	10.691	0.828	8.602	3.283	-1.828
	0.4		0.765	8.203	0.552	8.634	0.690	8.426	0.981	-1.281
	0.5		0.762	8.593	4.143	8.200	0.276	7.981	0.328	0.721
	0.6		0.820	9.375	5.800	7.597	0.276	7.386	-0.701	2.689
	0.7		0.921	8.984	8.010	6.451	0.276	6.667	-0.610	3.250
	0.8		1.039	8.593	11.048	4.140	0.552	6.058	-0.236	2.047
	0.85		1.070	-	-	-	0.000	5.659	-	0.914
	0.9		1.042	8.893	12.429	4.869	-	-	-0.354	-
	0.915		1.023	8.893	13.810	6.001	-	-	-0.295	-
	0.930		0.980	10.129	13.258	6.225	-	-	-0.622	-
	0.950		0.906	11.117	10.219	8.648	-	-	-2.441	-

TABLE II   (Cont...)

Streamwise station x_H	Spanwise location z/z_L	Gapwise location $\dfrac{r-r_o}{r_i-r_o}$	Streamwise mean veloc. $\bar{U}/V_c$	Streamwise turb.level $\tilde{u}/V_c$ $\times 10^2$	Gapwise mean veloc. $\bar{V}/V_c$ $\times 10^2$	Gapwise turb.level $\tilde{v}/V_c$ $\times 10^2$	Spanwise mean veloc. $\bar{W}/V_c$ $\times 10^2$	Spanwise turb.level $\tilde{w}/V_c$ $\times 10^2$	Cross-correlat. $-\overline{uv}/V_c^2$ $\times 10^3$	Cross-Correlat. $-\overline{uw}/V_c^2$ $\times 10^3$
+2.50	0.0	0.9	0.843	9.388	-12.429	5.310	-0.828	11.966	-1.441	0.217
	0.1		0.843	8.989	-12.153	5.744	-3.176	11.113	-1.259	3.173
	0.2		0.863	7.905	-8.562	6.066	-9.253	7.609	0.170	1.739
	0.3		0.947	6.917	-5.524	6.057	-11.877	6.058	1.269	0.476
	0.4		0.966	6.794	-1.381	6.057	-12.429	5.403	1.361	0.679
	0.5		0.982	6.794	1.104	6.041	-11.402	5.157	0.881	0.732
	0.6		0.998	6.670	3.590	5.914	-10.219	5.009	0.305	0.496
	0.7		1.021	7.041	6.352	5.932	-7.181	4.821	-0.721	0.000
	0.8		1.011	9.017	8.562	7.183	-5.901	5.291	-2.417	-0.965
	0.85		0.984	-	-	-	-4.213	5.719	-	-1.555
	0.9		0.843	10.156	6.905	8.467	-	-	-3.227	-
	0.915		0.812	10.546	5.524	7.974	-	-	-3.227	-
	0.930		0.777	10.546	3.590	7.974	-	-	-3.227	-
	0.950		0.722	11.328	2.485	7.238	-	-	-2.929	-

33

Table III. 90 DEGREE BEND OF 2.3 RADIUS RATIO AND SQUARE CROSS-SECTION
TURBULENT FLOW: REYNOLDS NUMBER 40 000
WALL PRESSURE MEASUREMENTS

Streamwise station θ (deg.)	Gapwise location $\dfrac{r-r_o}{r_i-r_o}$	Spanwise location $z/z_{\frac{1}{2}}$	Pressure coefficient $Cp = \dfrac{P-P_{ref}}{\frac{1}{2} V_c^2}$
0	0.0	0.0	0.000 (Pref)
	0.1	1.0	−0.019
	0.3	1.0	−0.098
	0.5	1.0	−0.133
	0.7	1.0	−0.278
	0.9	1.0	−0.379
45	0.0	0.0	0.174
	0.1	1.0	0.114
	0.3	1.0	−0.012
	0.5	1.0	−0.241
	0.7	1.0	−0.516
	0.9	1.0	−0.660
71	0.0	0.0	0.160
	0.1	1.0	0.092
	0.3	1.0	−0.055
	0.5	1.0	−0.251
	0.7	1.0	−0.516
	0.9	1.0	−0.637
90	0.0	0.0	−0.039
	0.1	1.0	−0.100
	0.3	1.0	−0.207
	0.5	1.0	−0.327
	0.7	1.0	−0.496
	0.9	1.0	−0.548

APPENDIX 2

DEFINITION OF SYMBOLS

Roman Characters

C_p	Pressure coefficient (figure 15)
De	Dean number: $De \equiv (\frac{\frac{1}{2}d}{R_c})^{1/2} Re$
d	Hydraulic diameter (40 mm)
k	Turbulent kinetic energy: $k \equiv \frac{1}{2}\rho(\tilde{u}^2 + \tilde{v}^2 + \tilde{w}^2)$
p	Pressure at wall
p_{ref}	Reference value of p ($\theta = 0^o$, $r^* = 0$, $z^* = 0$)
r	Radial co-ordinate direction (fig. 1)
r_i	Radius of curvature of suction surface
r_o	" " " " pressure "
Re	Reynolds number: $Re \equiv \frac{V_c}{\nu d}$
R_c	Mean radius of curvature: $R_c \equiv 0.5(r_i + r_o)$
r^*	Normalised radial co-ordinate: $r^* \equiv \frac{r - r_o}{r_i - r_o}$
U	Mean velocity in θ (streamwise) direction
$\tilde{u}$	R.m.s. fluctuating velocity in θ direction
$\overline{uv}$	Cross-correlation between $\tilde{u}$ and $\tilde{v}$
$\overline{uw}$	Cross-correlation between $\tilde{u}$ and $\tilde{w}$
V	Mean velocity in r (radial) direction
V_c	Bulk mean velocity
$\tilde{v}$	R.m.s. fluctuating velocity in r direction
W	Mean velocity in z (spanwise) direction

$\tilde{w}$ R.m.s. fluctuating velocity in z direction

X_H Axial distance along straight duct, expressed in hydraulic diameters

z Spanwise co-ordinate direction (fig. 1)

$z_{1/2}$ Duct half-width (20 mm)

z^* Normalised spanwise co-ordinate: $z^* \equiv \dfrac{z}{z_{1/2}}$

Greek Characters

θ Axial (streamwise) co-ordinate direction (fig. 1)

ν Kinematic viscosity of water

ρ Density of water

ϕ Half-angle of beam intersection

REFERENCES

1. Ward Smith, A.J. (1971). Pressure losses in ducted flows. Butterworths, London.
2. Rowe, M. (1970). Measurements and computations of flow in pipe bends. J. Fluid Mech., 43, 771.
3. Agrawal, Y., Talbot, L. and Gong, K. (1978). Laser anemometer study of flow development in curved circular pipes. J. Fluid Mech., 85, 497.
4. Mori, Y., Uchida, Y. and Ukon, T. (1971). Forced convective heat transfer in a curved channel with a square cross-section. Int. J. Heat Mass Transfer, 14, 1787.
5. Eskinazi, S. and Yeh, H. An investigation of fully-developed turbulent flows in a curved channel. J. Aero. Sci., 23, 23.
6. Bruun, H.H. (1979). An experimental investigation of secondary flow losses in bends with rectangular cross-sections. Univ. of Cambridge, Dept. of Eng. Report CUED/A-Turbo/TR 95.
7. Humphrey, J.A.C., Taylor, A.M.K. and Whitelaw, J.H. (1977). Laminar flow in a square duct of strong curvature. J. Fluid Mech., 83, 509.
8. Humphrey, J.A.C., Whitelaw, J.H. and Yee, G. (1980). Turbulent flow in a square duct with strong curvature. To be published in J. Fluid Mech.
9. Melling, A. and Whitelaw, J.H. (1976). Turbulent flow in a rectangular duct. J. Fluid Mech., 78, 289.
10. Taylor, A.M.K.P. (1980). Confined isothermal and combusting flows behind axisymmetric baffles. Ph.Thesis, University of London.
11. Durst, F., Melling, A. and Whitelaw, J.H. (1976). Principles and practice of laser Doppler anemometry. Academic Press, London.
12. Johnston, J.P. (1976) Internal flows. Bradshaw, P. (ed). Turbulence. Springer-Verlag, Berlin.
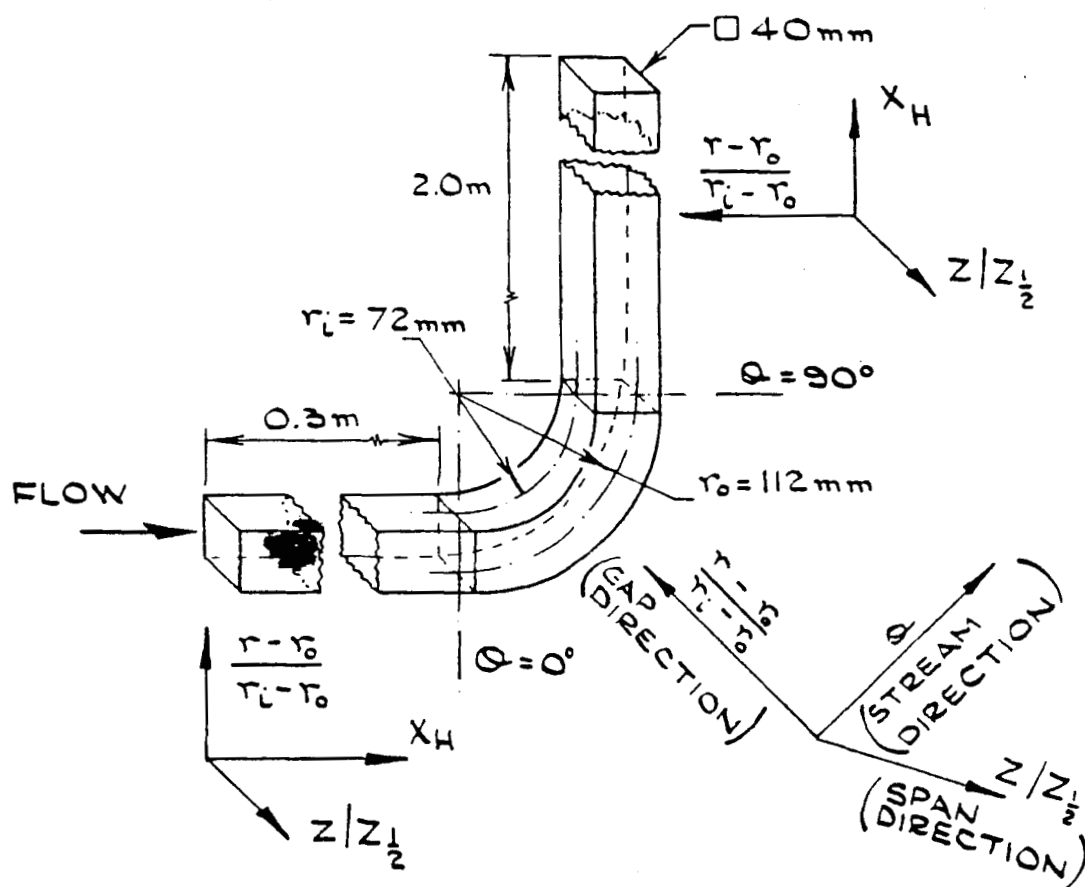
Fig. 1   Dimensions of bend and co-ordinate

definition sketch.
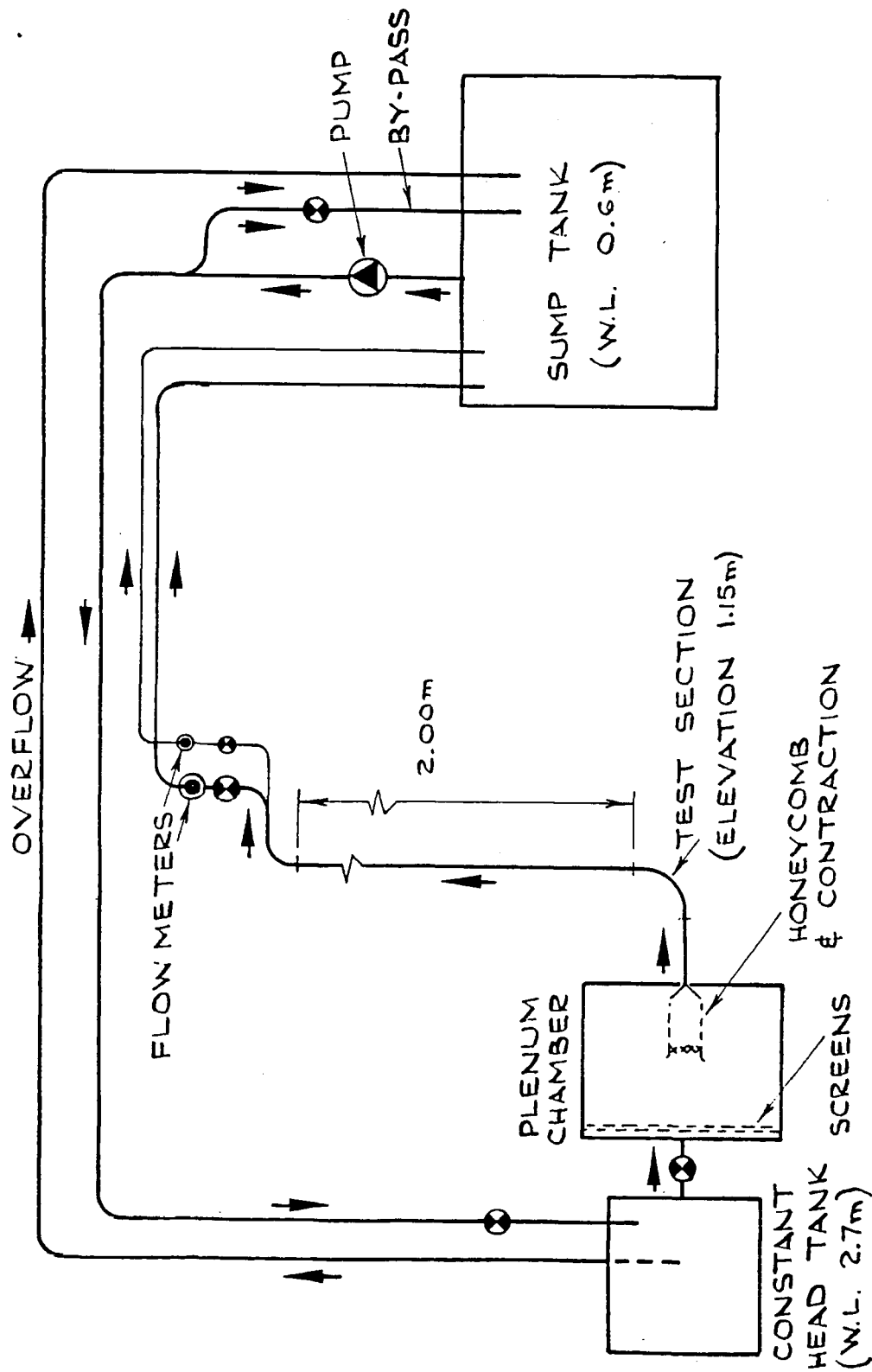
Fig. 2 Plan view of water-tunnel.

PUMP

BY-PASS

SUMP TANK
(W.L. 0.6m)

OVERFLOW

FLOW METERS

2.00m

TEST SECTION
(ELEVATION 1.15m)

HONEYCOMB
& CONTRACTION

PLENUM
CHAMBER

SCREENS

CONSTANT
HEAD TANK
(W.L. 2.7m)
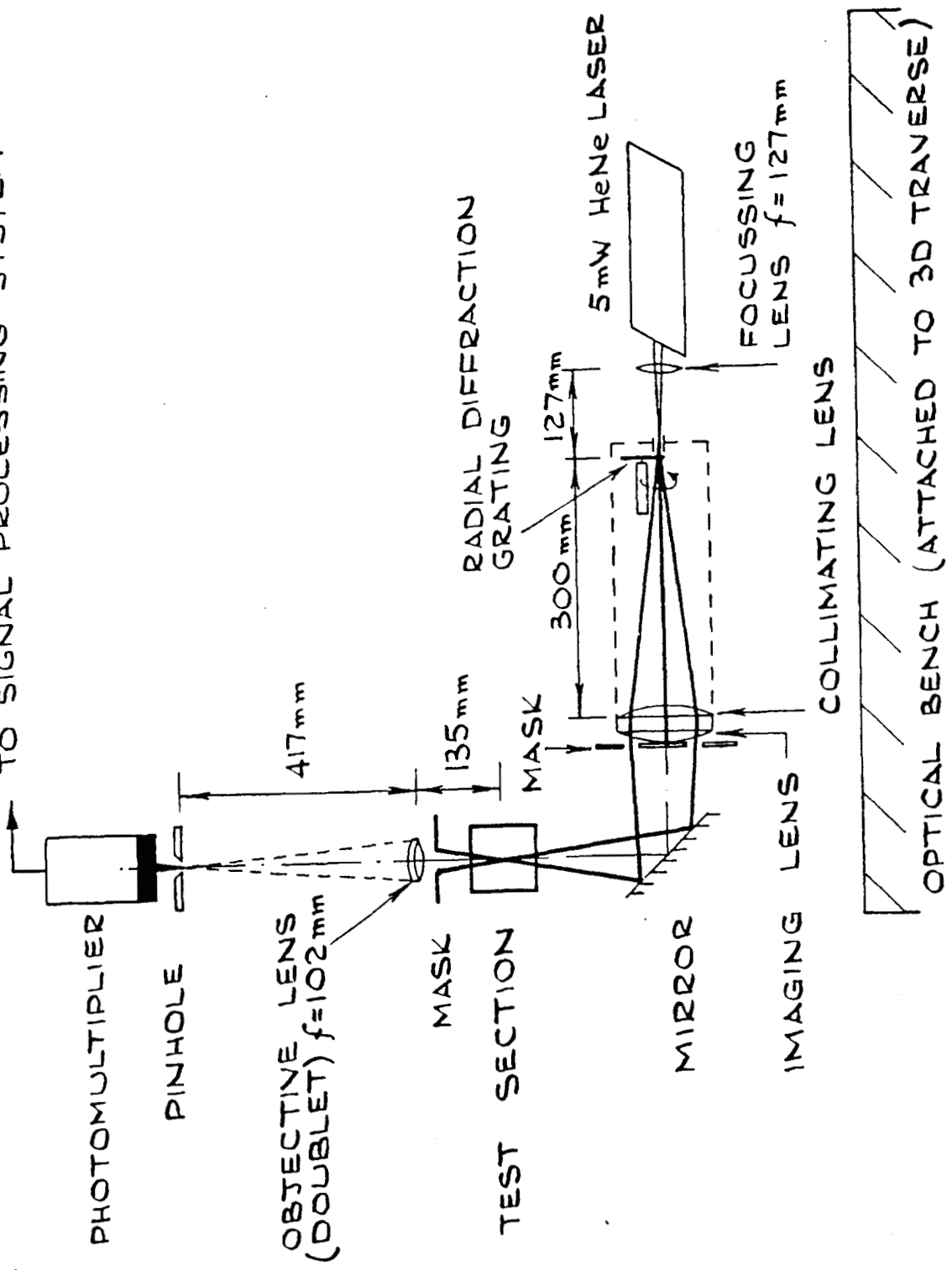
Fig. 3(i)   Optical arrangement of laser-Doppler velocimeter.

40
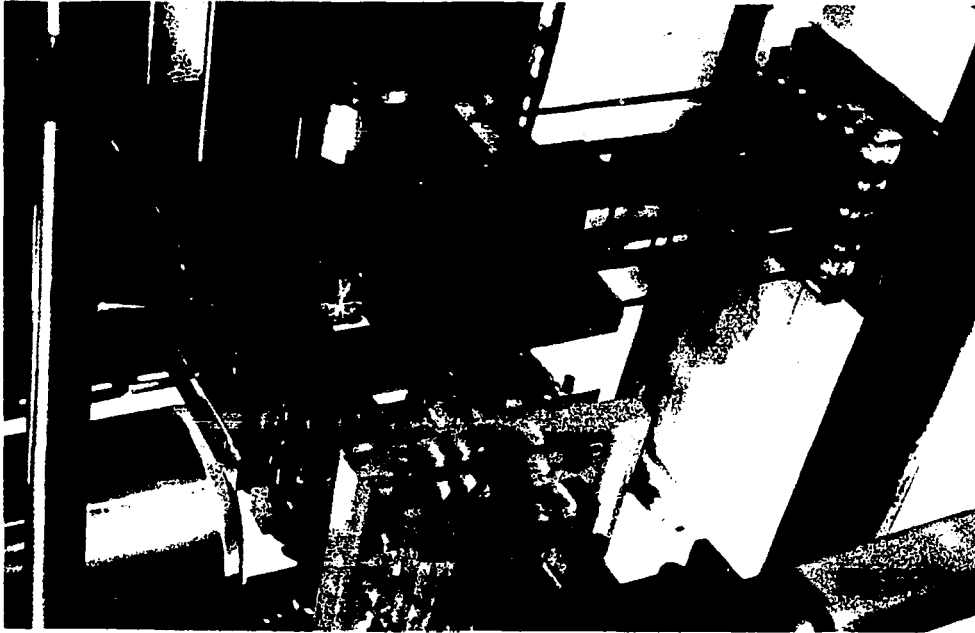
Fig. 3(ii)   View of bend showing intersection volume.

Fig. 3(iii)   View of optical system.
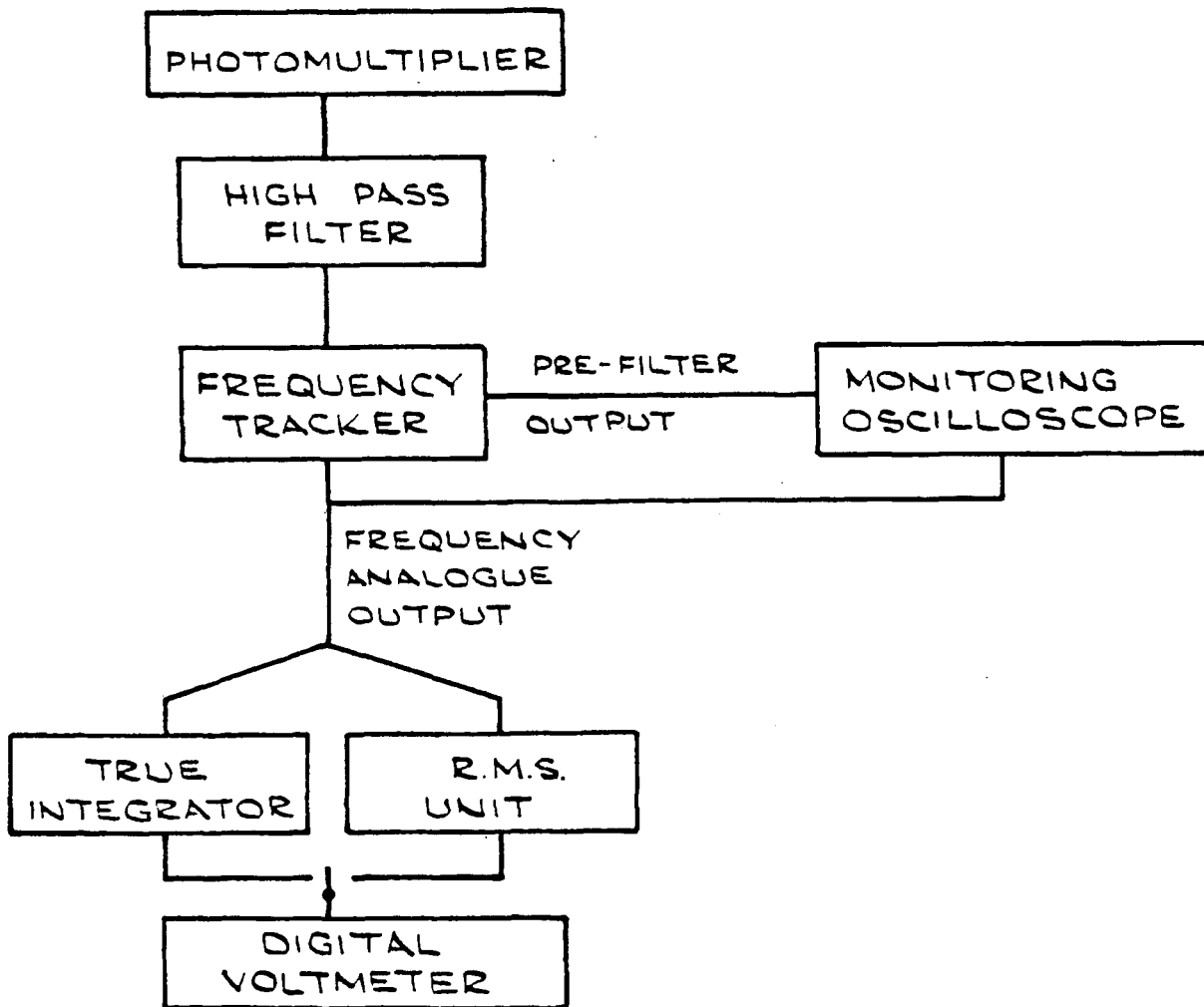
Fig. 4 Block diagram of Doppler signal processing
arrangement.
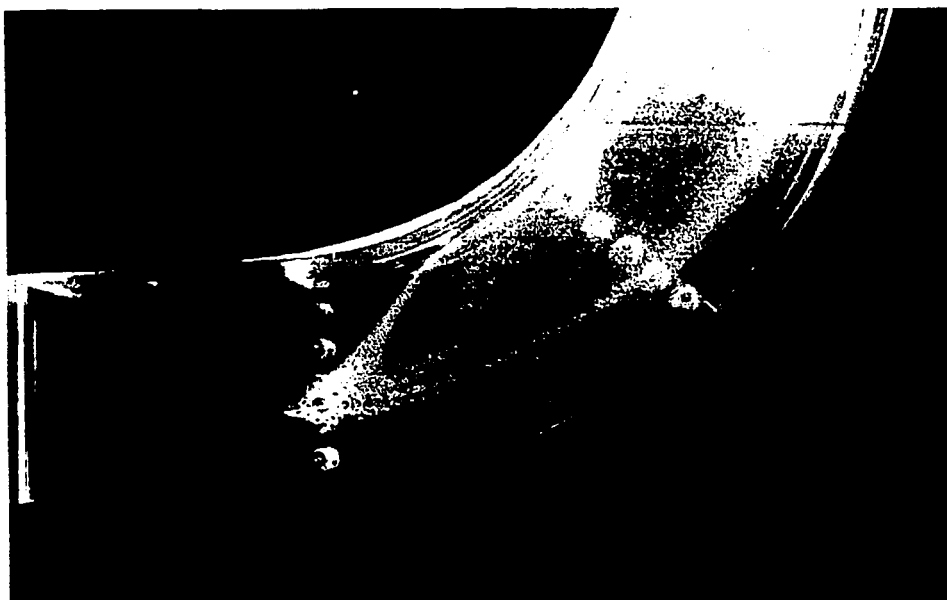
Fig. 5(i)   Visualization of secondary flow at entrance to the bend.
Re = 1275. Flow direction from left to top right;
Wire inserted at $\theta = 0^{\circ}$, $r^* = 0.3$.

Fig. 5(ii)   Visualization of flow at exit of the bend. Re = 790.
Flow direction from left to top right; wires inserted
at $\theta = 71^{\circ}$, $r^* = 0.1$, 0.5 and 0.9.
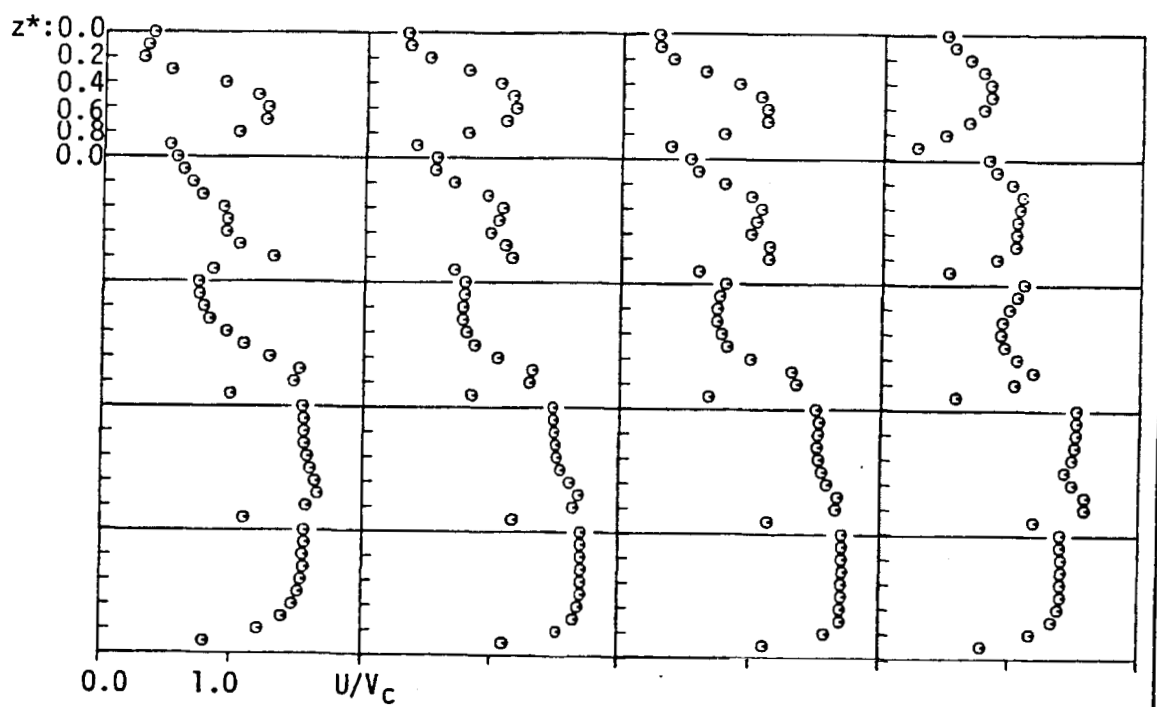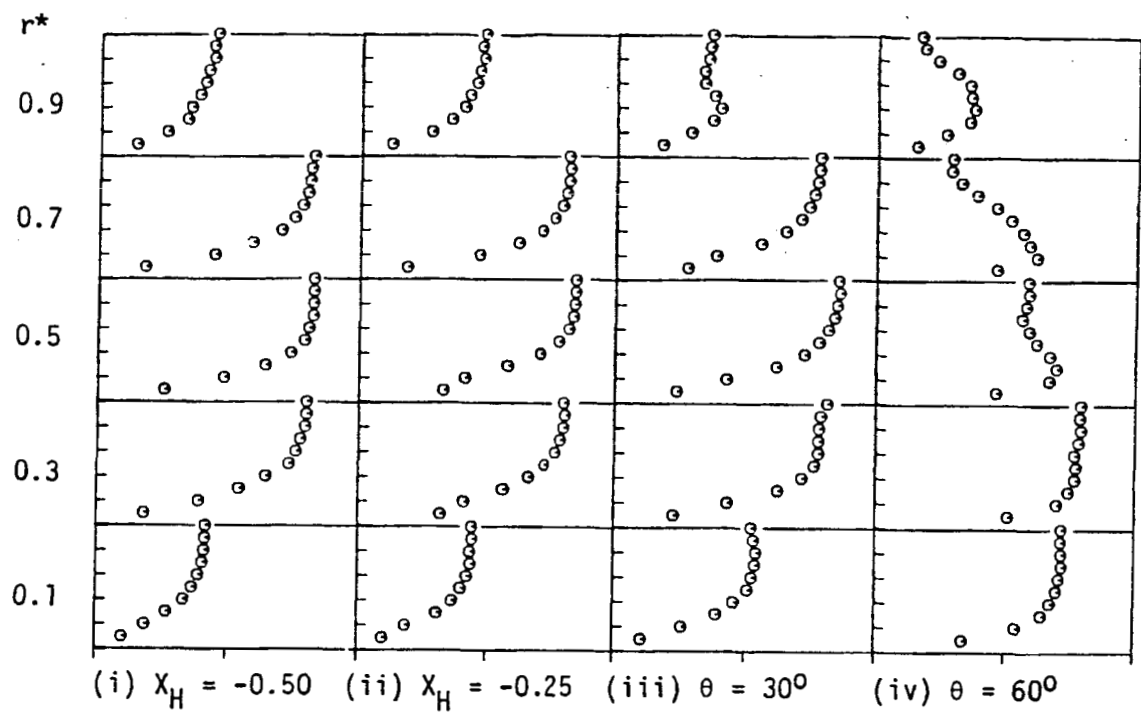
Fig. 6   Laminar flow: profiles of U/V_c at successive streamwise stations.
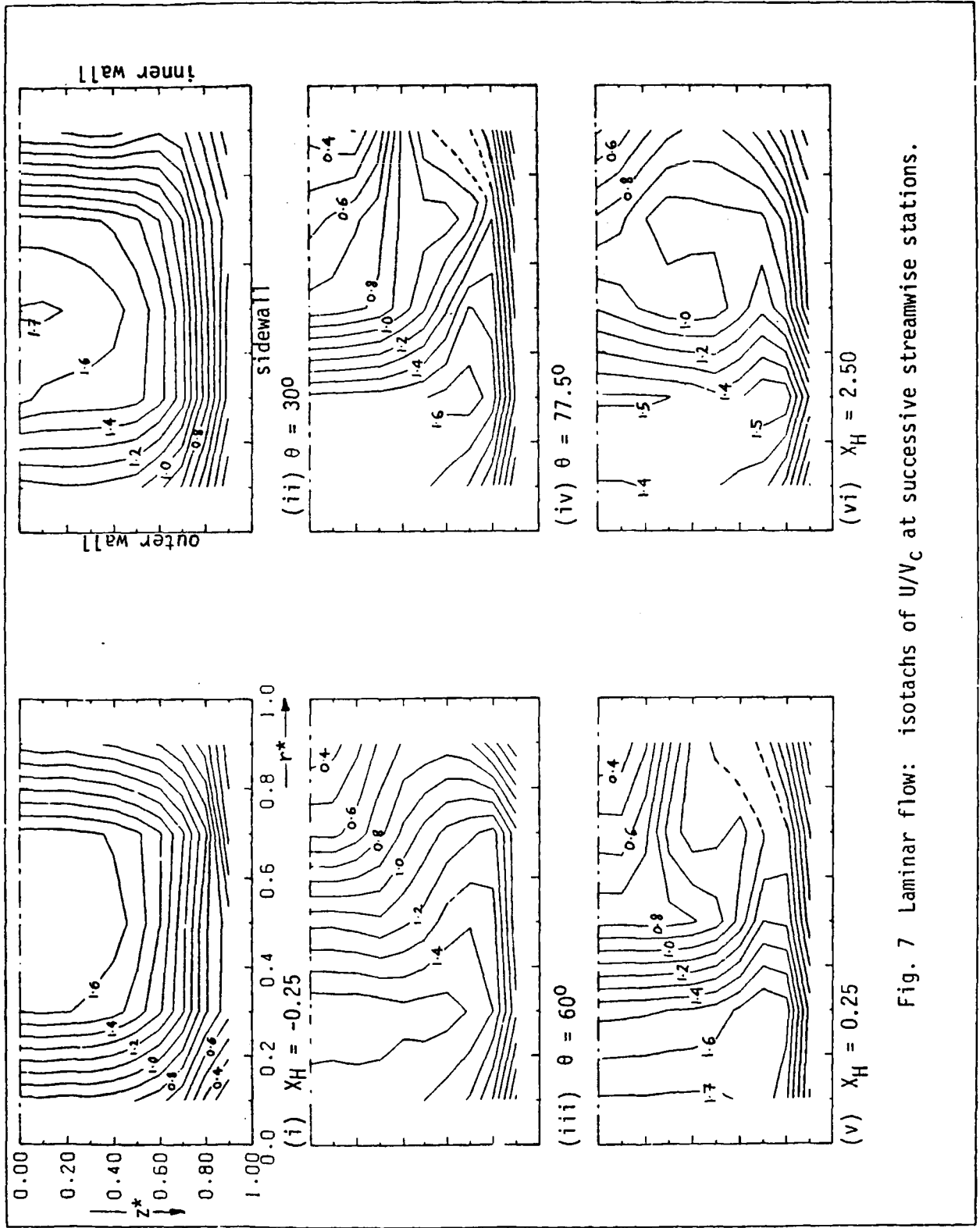
Fig. 7 Laminar flow: isotachs of U/V_C at successive streamwise stations.

Fig. 8   Laminar flow: profiles of V/V_c at successive streamwise stations.

(i) $X_H = -0.25$

(ii) $\theta = 30^0$

(iii) $\theta = 60^0$

(iv) $\theta = 77.5^0$

(v) $X_H = 0.25$

(vi) $X_H = 2.50$

inner wall

sidewall

outer wall
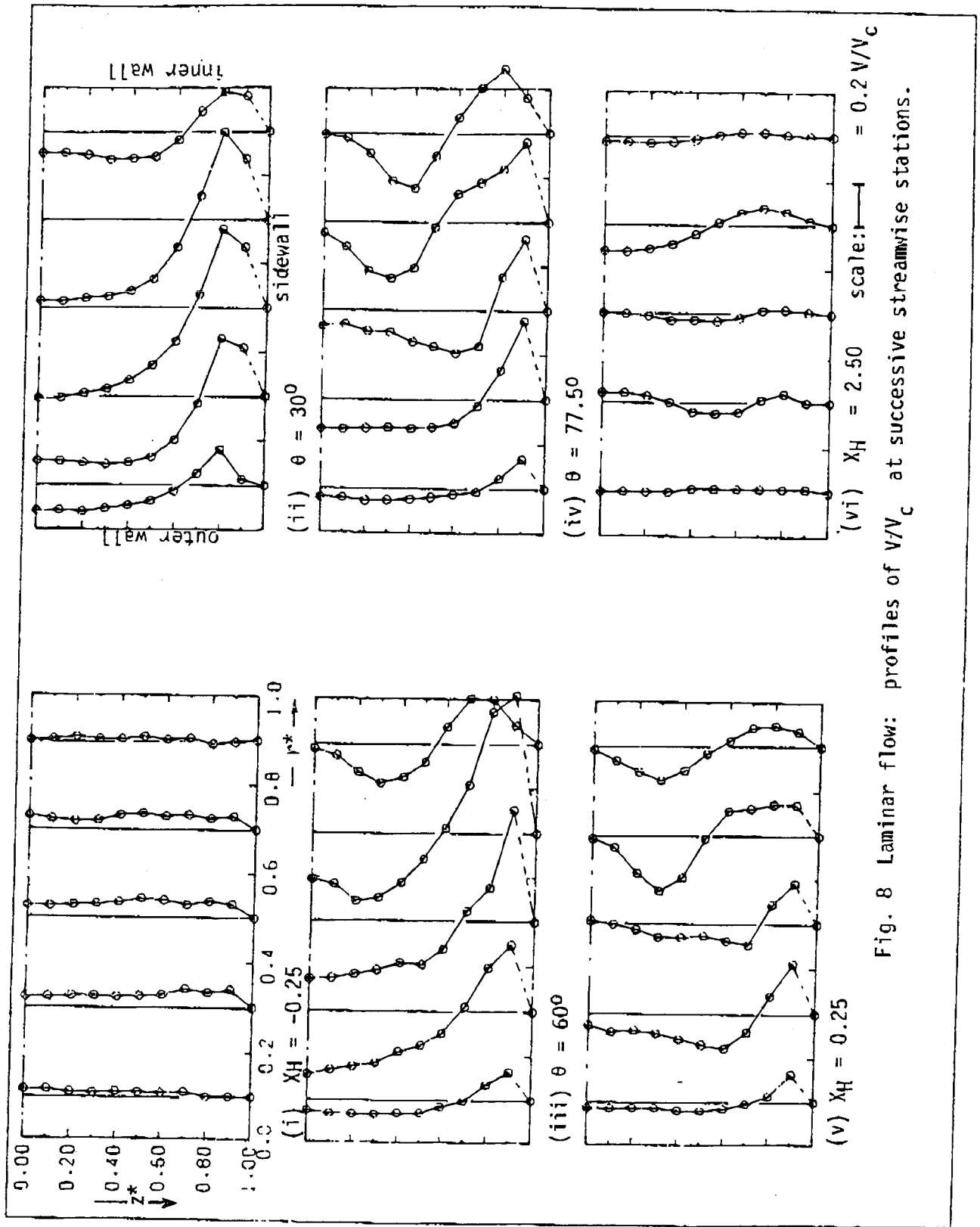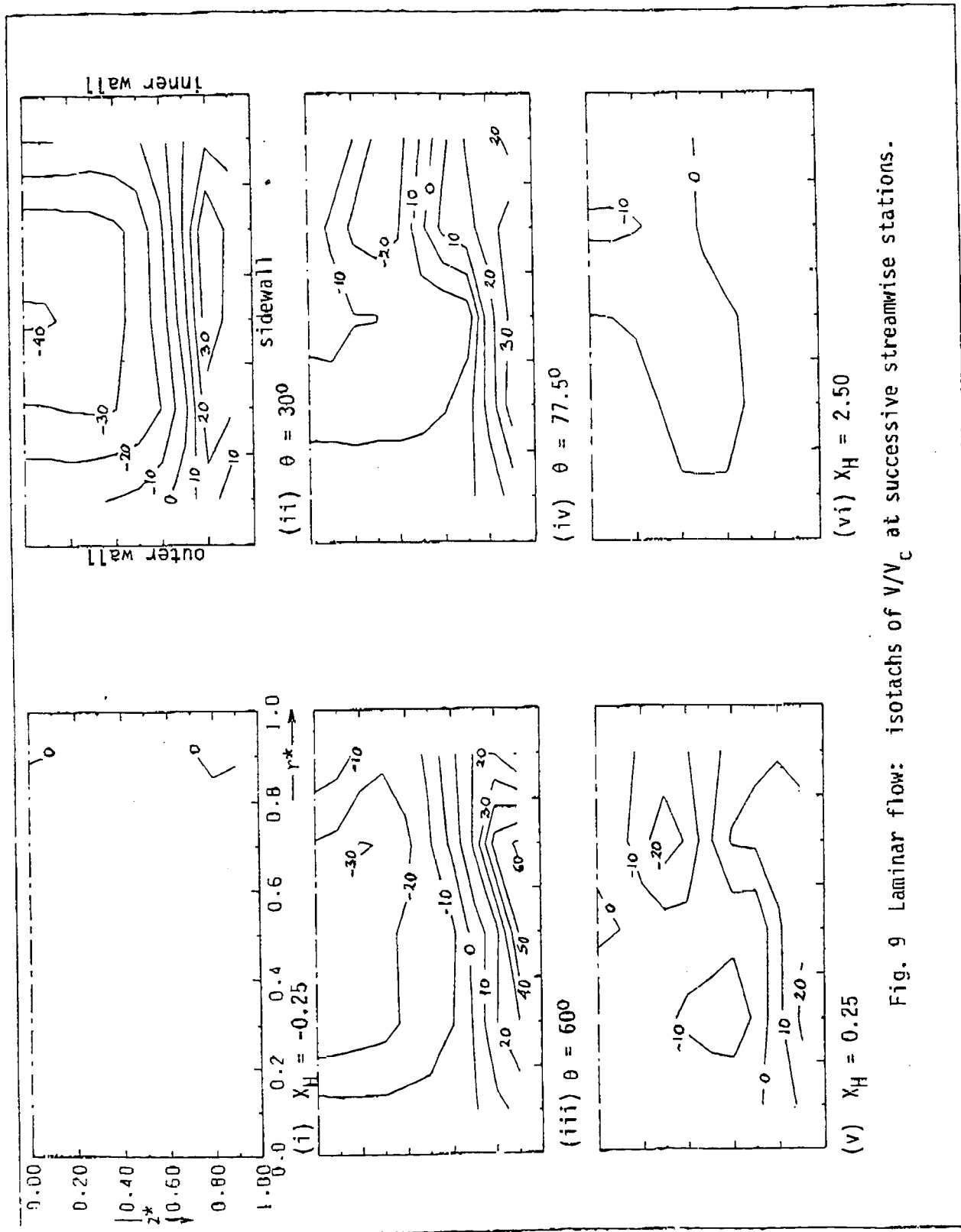
Fig. 9 Laminar flow: isotachs of V/V_c at successive streamwise stations.

: direction of positive W

scale: $\longmapsto$ = 0.20 W/V_c
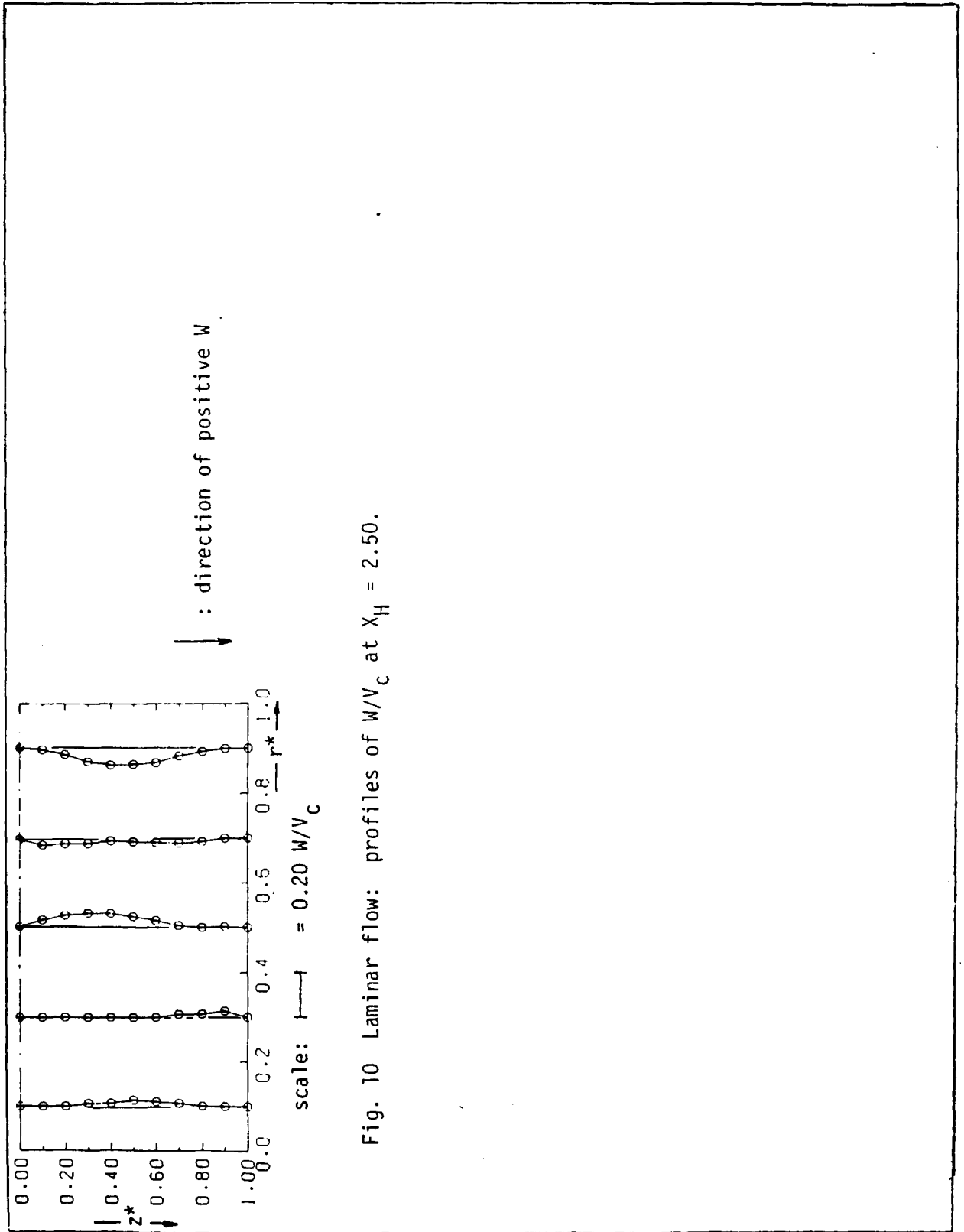
Fig. 10 Laminar flow: profiles of W/V_c at X_H = 2.50.
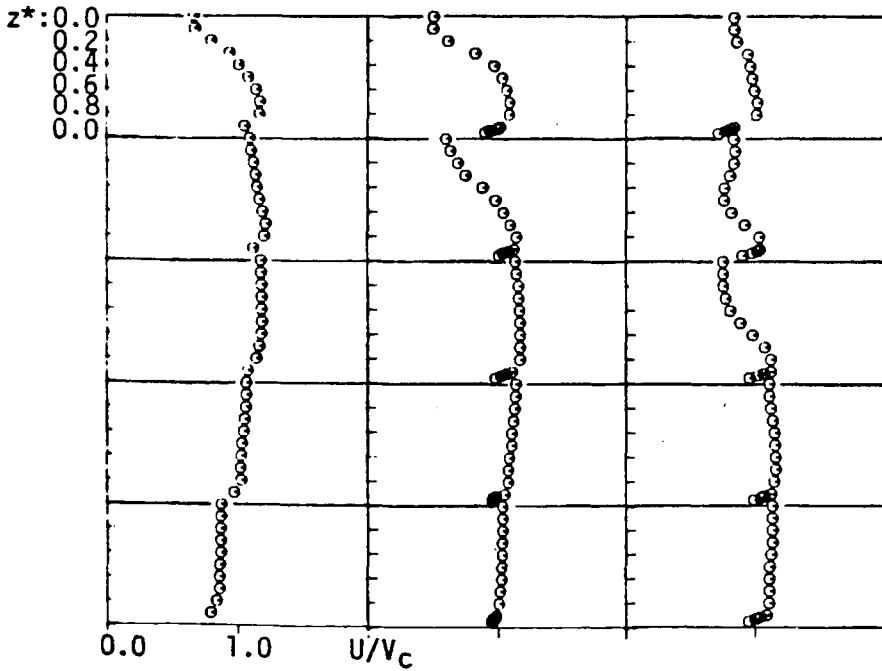
Fig.11   Turbulent flow: profiles of U/V_c at successive
         streamwise stations.
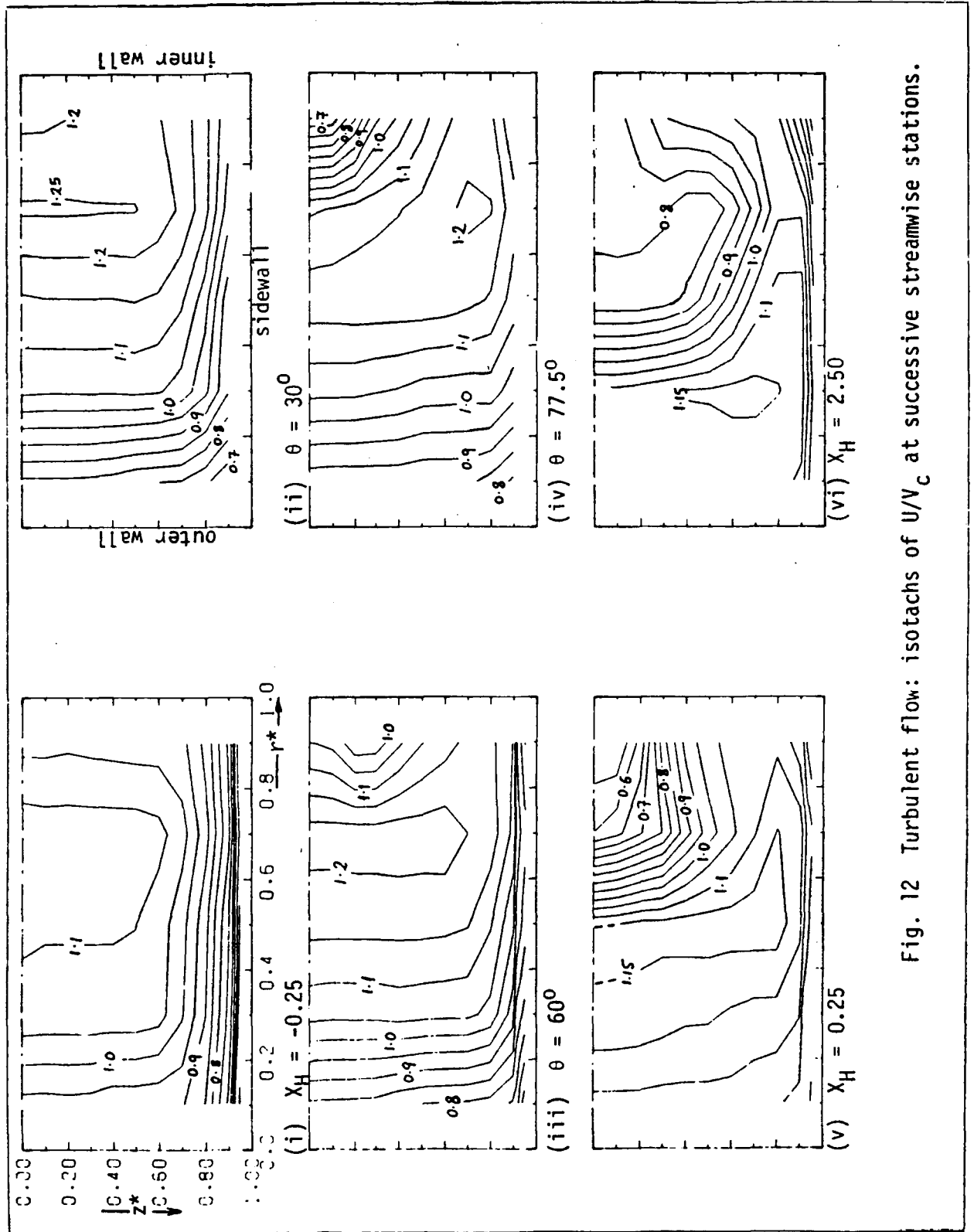
Fig. 12 Turbulent flow: isotachs of U/V_c at successive streamwise stations.
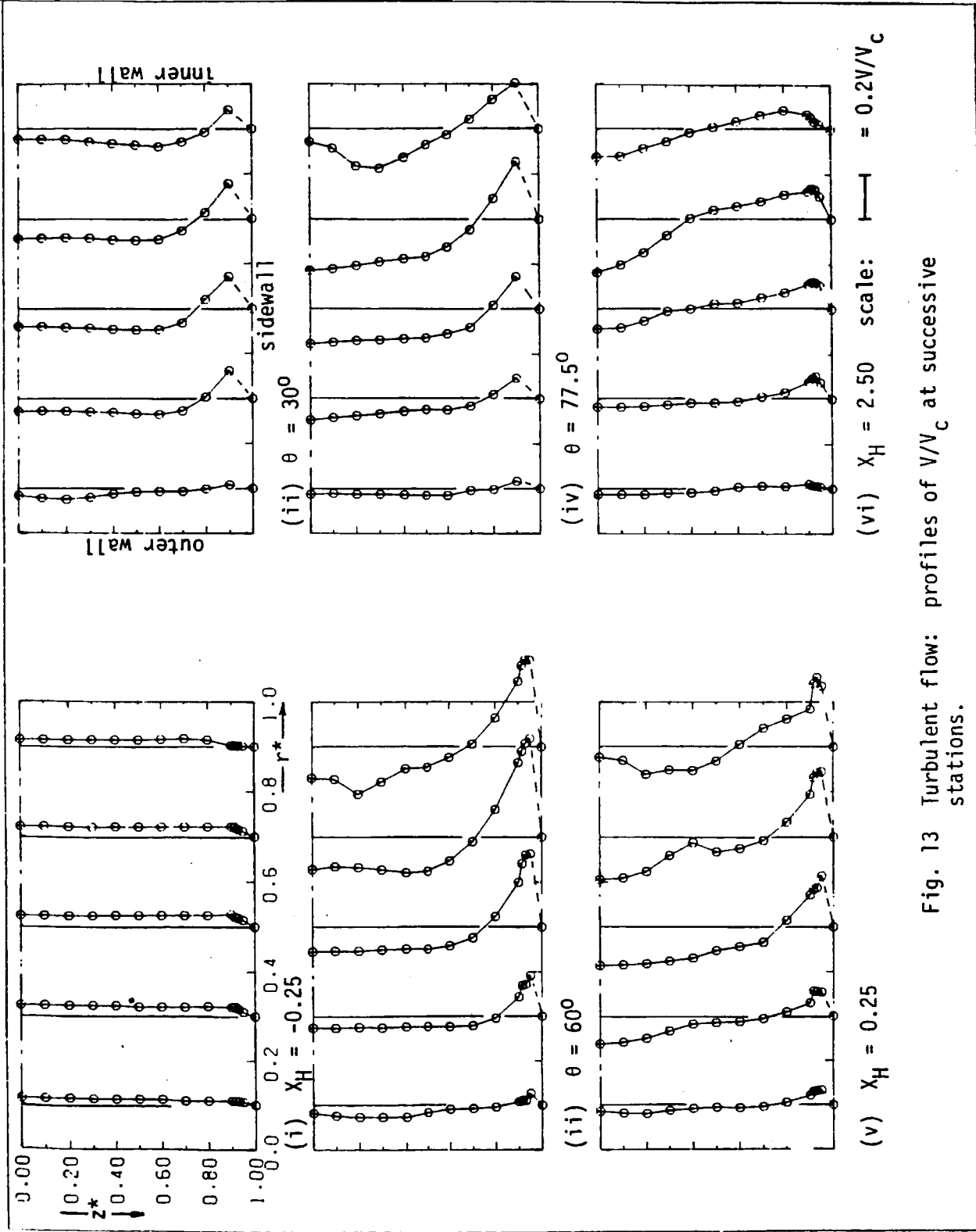
Fig. 13 Turbulent flow: profiles of V/V_c at successive stations.
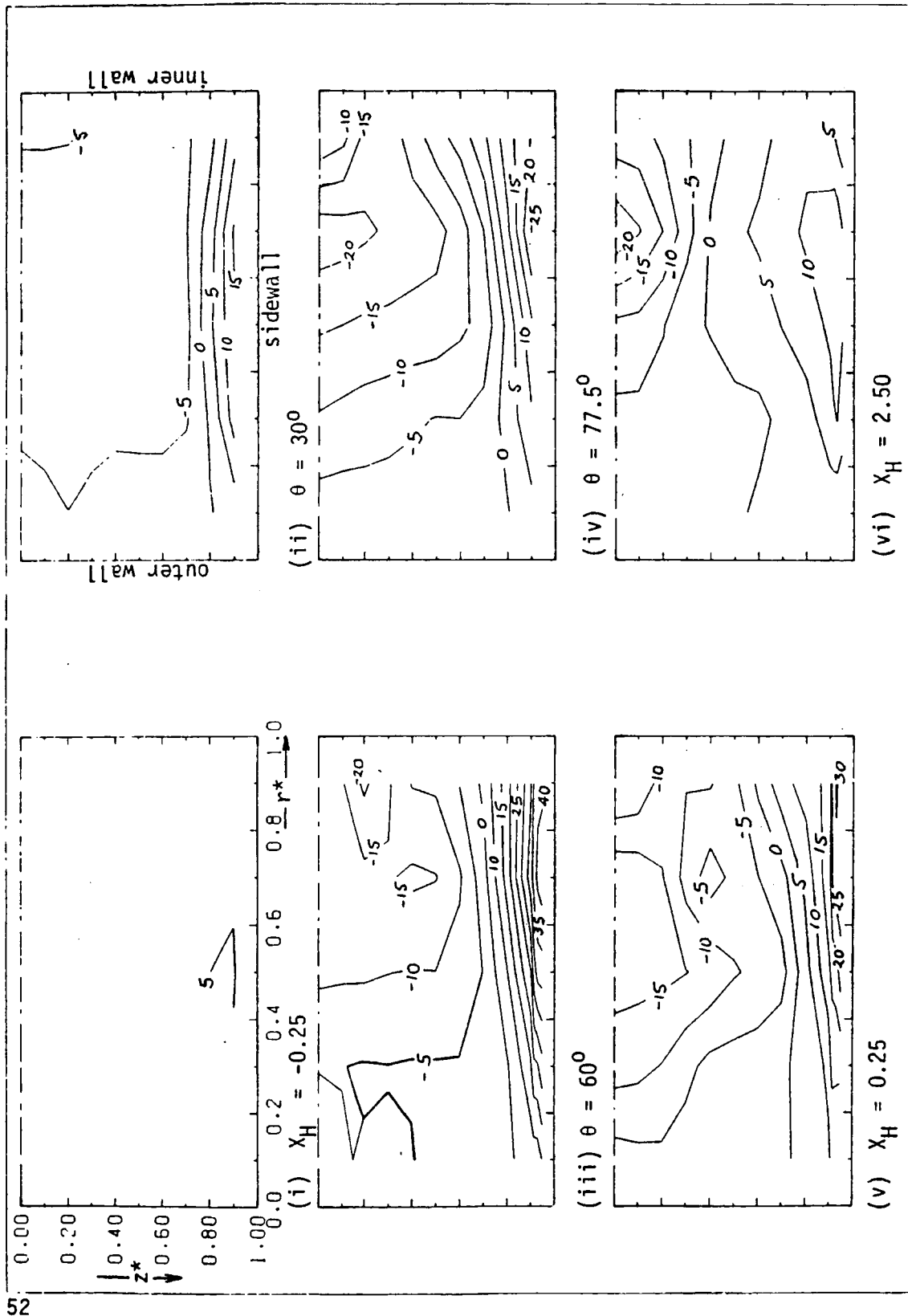
Fig. 14 Turbulent flow: isotachs of V/V_c at successive streamwise stations.

(ii) Gapwise distribution

$Cp = (P - P_{ref})/\frac{1}{2}e V_c^2$
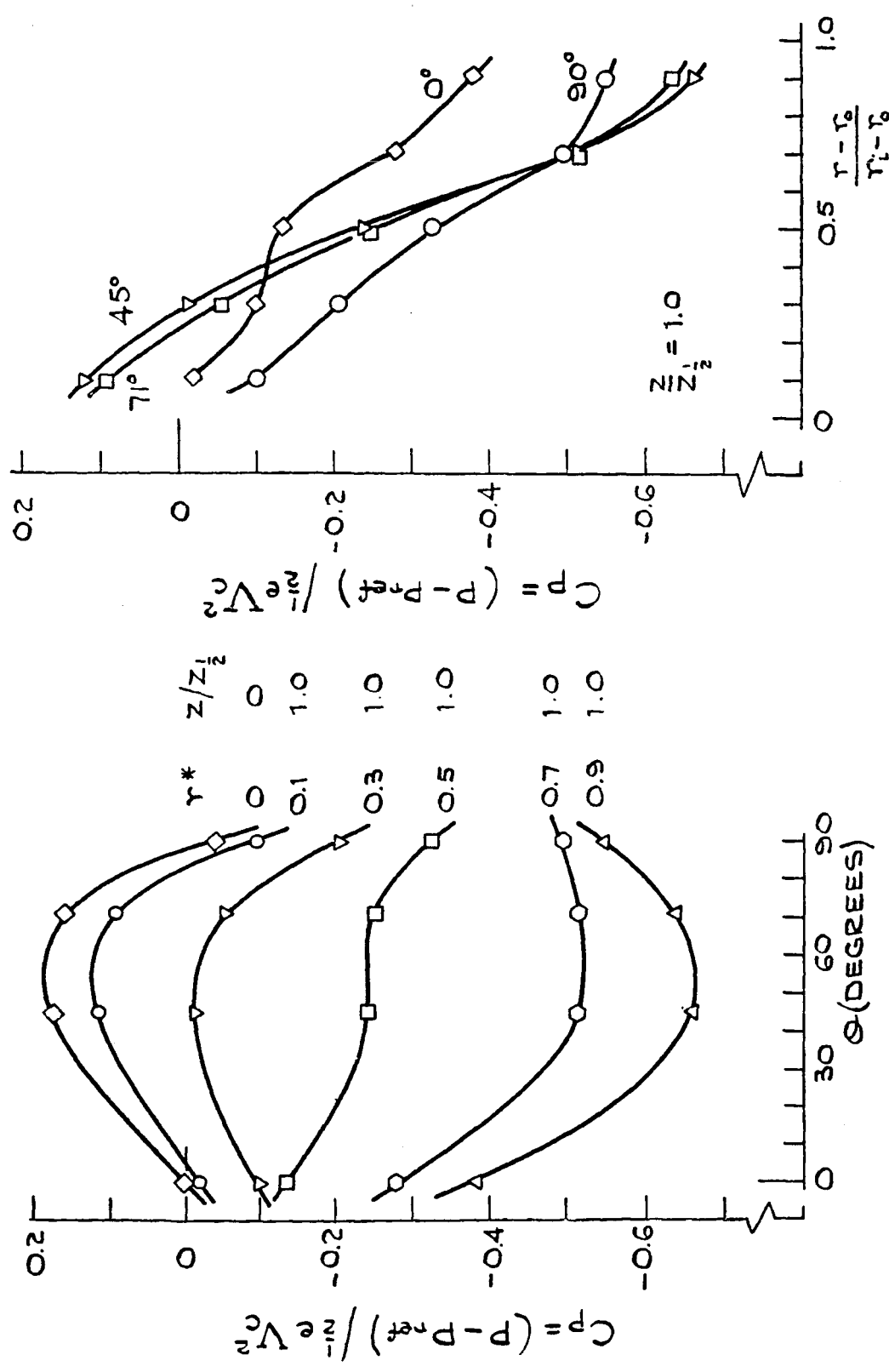
(i) Streamwise distribution

Fig. 15 Turbulent flow: wall static pressure measurements

53
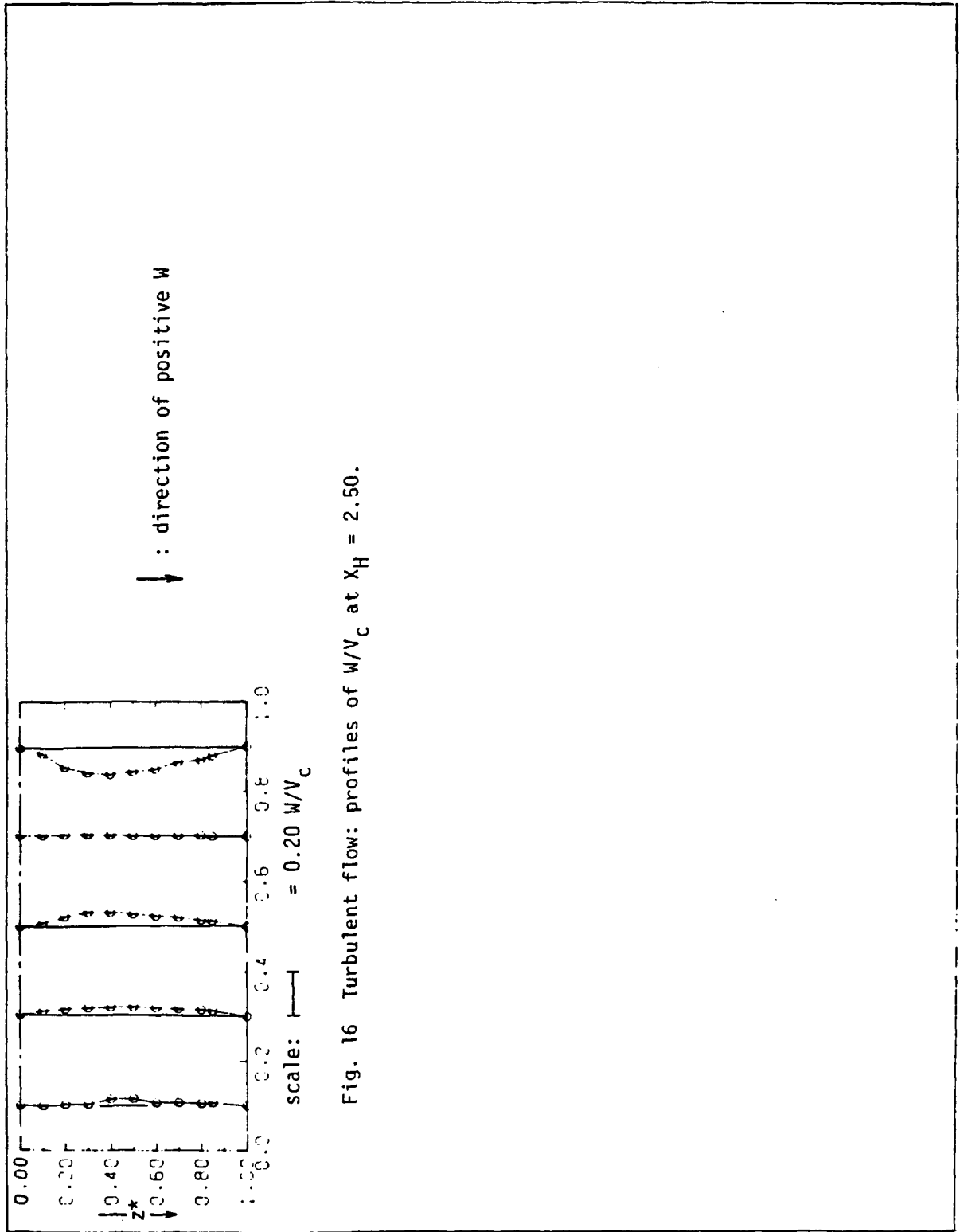
Fig. 16 Turbulent flow: profiles of W/V_C at X_H = 2.50.
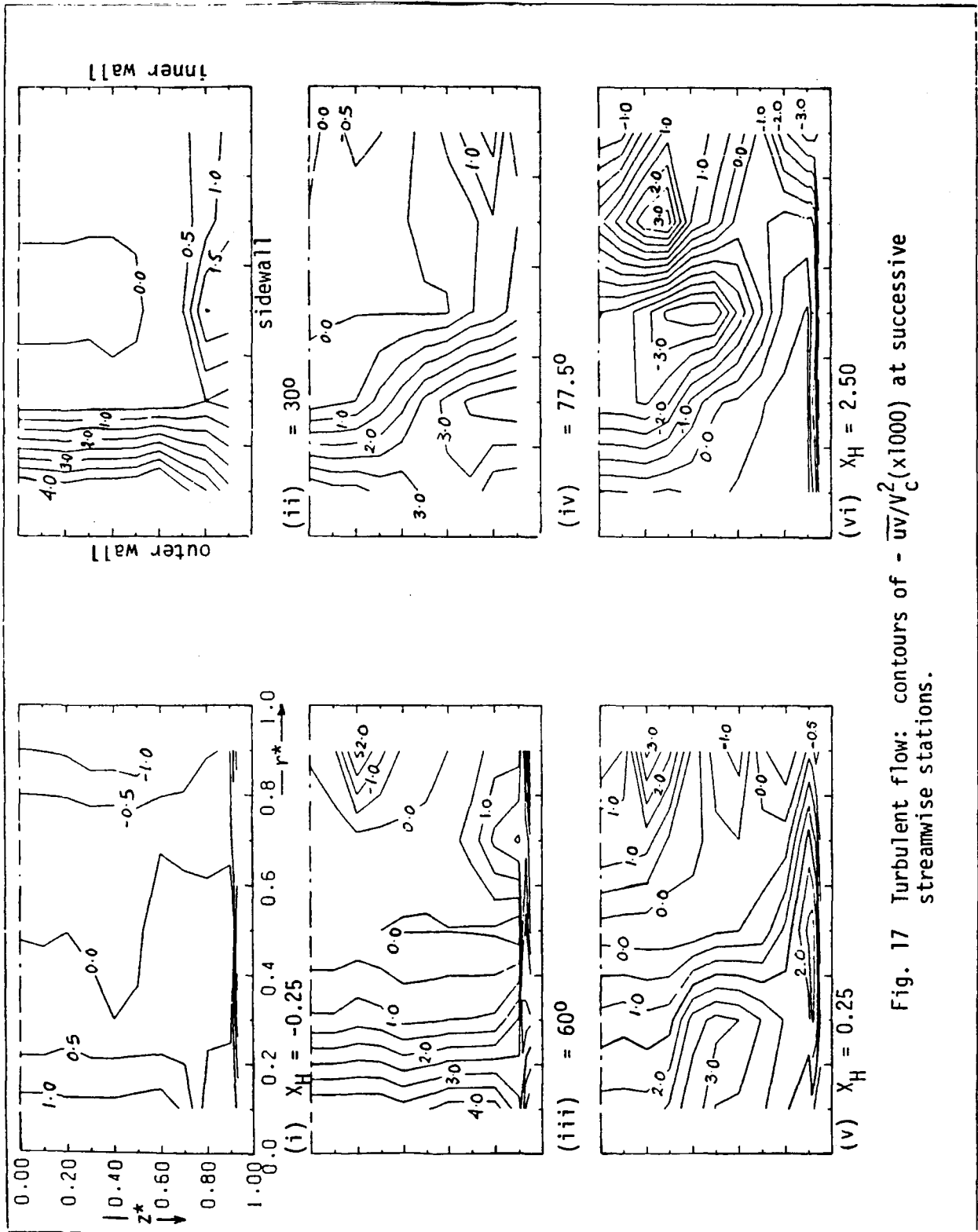
Fig. 17 Turbulent flow: contours of $-\overline{uv}/V_c^2(\times 1000)$ at successive streamwise stations.
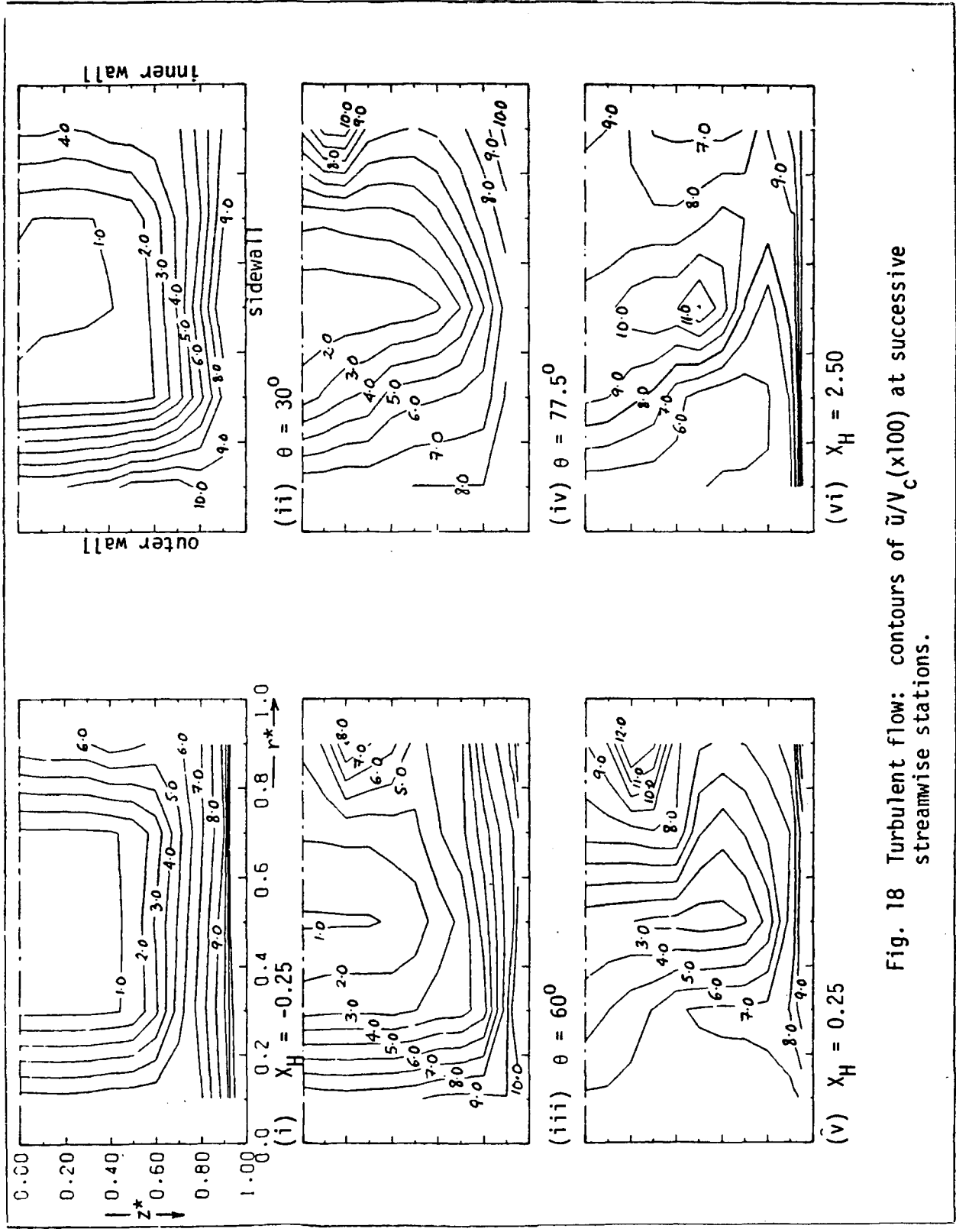
Fig. 18 Turbulent flow: contours of $\bar{u}/V_c$ (×100) at successive streamwise stations.

(i) $X_H = -0.25$

(ii) $\theta = 30°$

(iii) $\theta = 60°$

(iv) $\theta = 77.5°$

(v) $X_H = 0.25$

(vi) $X_H = 2.50$
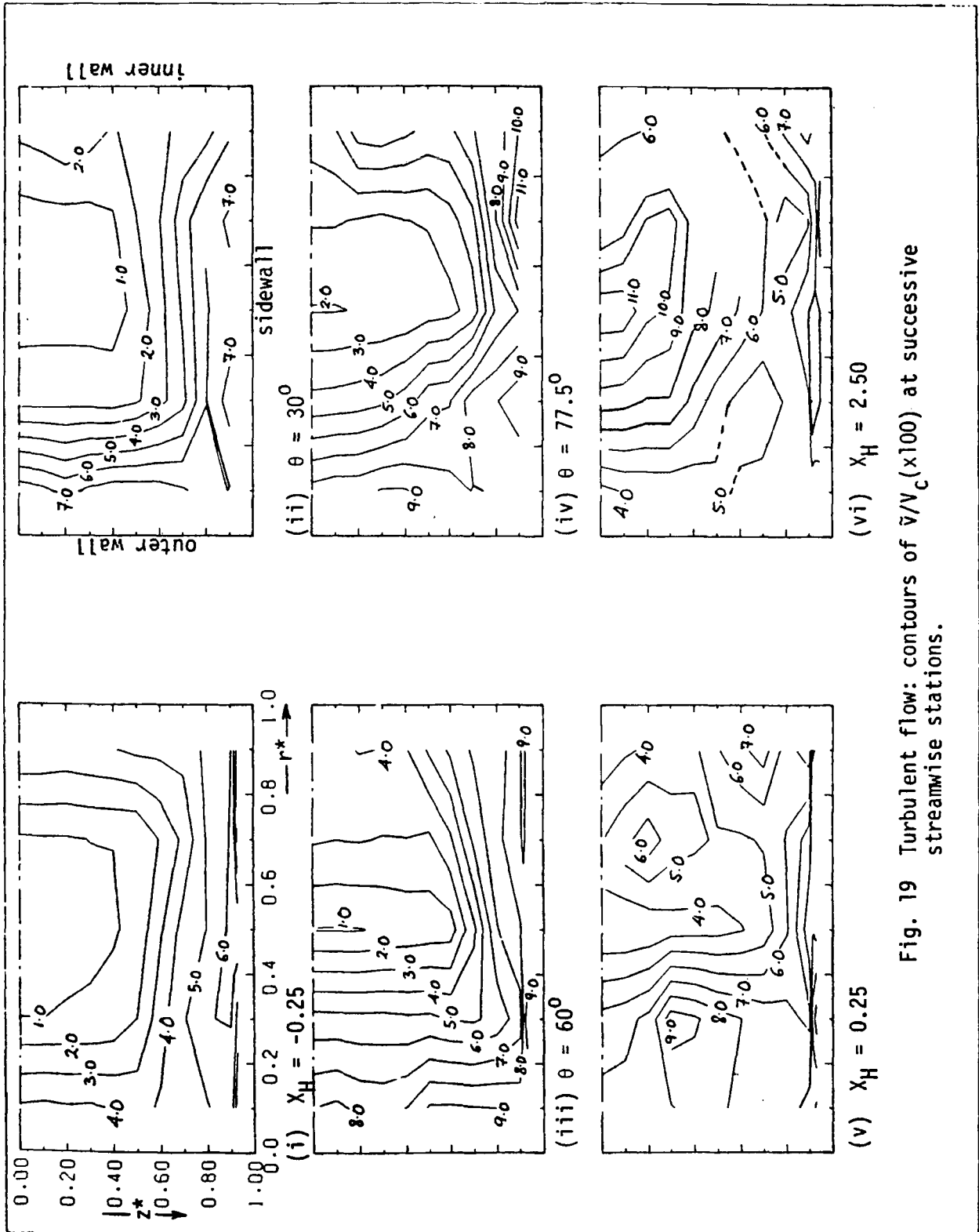
Fig. 19 Turbulent flow: contours of $\tilde{v}/V_c(\times 100)$ at successive streamwise stations.
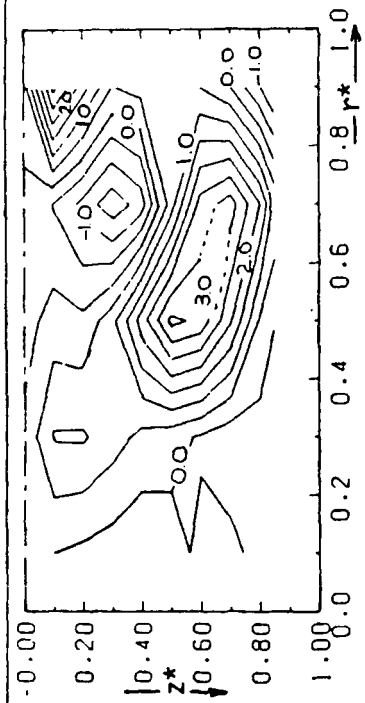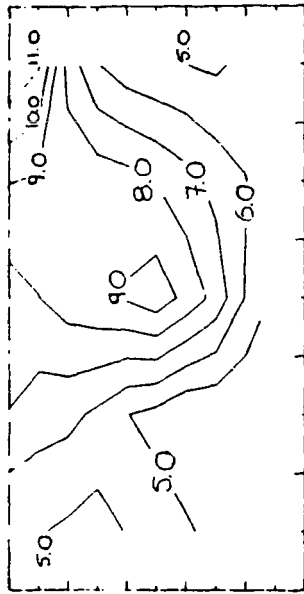
Fig. 21 Turbulent flow: contours of $\tilde{w}/V_c(\times 100)$ at $X_H = 2.50$.
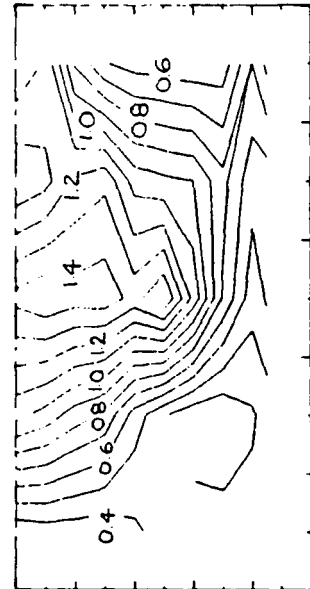
Fig. 22 Turbulent flow: contours of $k/V_c^2(\times 100)$ at $X_H = 2.50$.

Fig. 20 Turbulent flow: contours of $-\overline{uv}/V_c^2(\times 1000)$ at $X_H = 2.50$.